Numerical study of external explosion in vented hydrogen explosions

Shengchao Rui [a], Jianjun Xiao [a,*], Changjian Wang [b,c], Fangnian Wang [a], Mike Kuznetsov [a], Thomas Jordan [a]

[a] Institute of Thermal Energy Technology and Safety (ITES), Karlsruhe Institute of Technology (KIT), Germany
[b] School of Civil Engineering, Hefei University of Technology, Hefei, Anhui 230009, PR China
[c] Anhui International Joint Research Center on Hydrogen Safety, Hefei 230009, PR China

ARTICLE INFO

Keywords:
Vented explosion
External explosion
Hydrogen
Safety
GASFLOW-MPI

ABSTRACT

In the current study, numerical study of vented hydrogen explosions was performed utilizing computational fluid dynamics (CFD) software GASFLOW-MPI. A turbulent combustion model based on Schmidt correlation was formulated. Within this model, flame instabilities resulted from two intrinsic effects, Hydrodynamic instability, and Landau-Darrieus and Thermal-Diffusive instabilities were incorporated. The numerical simulation results revealed the mechanism of overpressure evolution inside and outside the vessel. Notably, the mechanism of the overpressure peak induced by the external explosion was revealed. The effects of turbulence models on overpressure time profiles were investigated. Moreover, it was determined that heat transfer, arising from thermal radiation and convection, exerts only a negligible influence on the maximum internal overpressure. Subsequently, the performance of GASFLOW-MPI in simulating vented hydrogen explosions for different ignition locations (center and rear ignitions) and varying hydrogen concentrations (22 %-38 %) was assessed against experimental data. Comparative analysis revealed a close agreement between the predicted results and experimental data. Furthermore, the competency of GASFLOW in simulating medium-scale vented hydrogen explosions was validated against experimental data.

1. Introduction

Due to the lower minimum ignition energy, higher diffusion and combustion rates, hydrogen deflagrations represent a predominant hazard within the hydrogen industry (Molkov, 2012). This hazard is inherent in confined spaces encountered during the production, transportation, and storage of hydrogen. However, vented hydrogen explosions have emerged as an effective and cost-effective technology, extensively investigated through experimental studies (Bauwens and Dorofeev, 2014; Cao et al., 2021; Kuznetsov et al., 2015; Li et al., 2019; Wang et al., 2022; Xu et al., 2022; Zhang et al., 2022, 2020). In recent years, the external overpressure has also been investigated during the vented hydrogen explosions due to the recognition of their significant impact on deflagration behavior (Guo et al., 2015; Kuznetsov et al., 2015; Mogi et al., 2017).Several empirical and semi-empirical engineering models were derived from theoretical deduction and then assessed using experimental data, these models provide a fast and economical means of characterizing the correlation between vent area and maximum reduced explosion overpressure (Bauwens et al., 2010, 2012b; Molkov and Bragin, 2015; Sinha et al., 2019; Sinha and Wen, 2019). However, the practical applicability of these engineering models is constrained to simple cases. Computational Fluid Dynamics (CFD) stands out as a precise and systematic method for predicting overpressure histories and flame evolution both inside and outside the vessel. The substantial development in computer technology now enables three-dimensional numerical simulations of hydrogen explosions (Xiao et al., 2017a, 2017b, 2016b). The physics underlying vented hydrogen explosions encompass laminar combustion, transitions from laminar to turbulent combustion, jet flame ignition, and heat and mass transfer. Consequently, overpressure histories and flame evolution in vented hydrogen explosions are subject to multiple influencing factors, including hydrogen concentration, vent area, and ignition location. Apart from circumventing risks and realizing substantial savings in personnel and material costs compared to experimental endeavors, numerical simulations furnish a more detailed depiction of the flow field. Numerical simulations facilitate a comprehensive understanding of the

* Correspondence to: Institute of Thermal Energy Technology and Safety (ITES), Karlsruhe Institute of Technology (KIT), Hermann-von-Helmholtz-Platz 1, Eggenstein-Leopoldshafen 76344, Germany.
E-mail address: jianjun.xiao@kit.edu (J. Xiao).

Table 1
Turbulence and combustion models used in FLACS, CFX, FLUENT and ADREA-HF.

Code	Turbulent model	Combustion model	Correlation
FLACS	k-ε	β-model(Arntzen, 1998)	$S_u = \max(S_{QL}, S_t)$ $S_{QL} = S_L\left(1 + c\cdot\min\left(\left(\frac{r_f}{3}\right)^{0.5}, 1\right)\right)$ $S_t = 1.81u'^{0.412}l_t^{0.196}S_L^{0.784}\mu^{0.196}$
CFX	k-ε	Zimont model	$S_t = AGu'^{3/4}S_L^{1/2}\lambda_u^{1/4}l_t^{1/4}$ $A = 0.5$
FLUENT	RNG LES	Multi-phenomena turbulent combustion model	$S_t = \Xi_k\cdot\Xi_{lp}\cdot\Xi_f\cdot\Xi_{RT}\cdot S_L\cdot\exp\left(\frac{u'}{S_t}\right)^2$
ADREA-HF	RNG LES	Multi-phenomena turbulent combustion model	$S_t = \Xi_k\cdot\Xi_{lp}\cdot\Xi_f\cdot\Xi_{RT}\cdot S_L\cdot\exp\left(\frac{u'}{S_t}\right)^2$

S_{QL}-quasi-laminar flame speed (m/s) ; S_t-turbulent flame speed(m/s) ; S_L-laminar flame speed (m/s) ; r_f -flame radius(m) ; u'-turbulent fluctuation velocity (m/s) ; l_t-characteristic length scale (m) ; μ-kinetic viscosity (kg/m/s) ; λ_u-thermal diffusion efficient for unburned gas (m^2/s) ; l_t-turbulent length scale (m) ; Ξ_k-wrinkling factor account for flame front itself ; Ξ_{lp}-wrinkling factor account for flame leading point ; Ξ_f-factor account for flame fractal ; Ξ_{RT}-factor account for Rayleigh-Taylor instability.

mechanisms governing overpressure escalation both inside and outside the vessel, elucidating the formation of the overpressure peaks.

In recent years, various Computational Fluid Dynamics (CFD) codes have been developed, each grounded in distinct turbulence and combustion models. The performance of these codes has been rigorously assessed through comparisons with certain experimental data. For instance, Bauwens et al. (2011) conducted numerical simulations of a vented hydrogen explosion within a 63.7 m^3 chamber, focusing on 18 % hydrogen-air mixtures. The CFD software employed was derived from the open-source platform *OpenFOAM*, utilizing the *PISO* algorithm (ISSA, 1985). Turbulence resolution was resolved using Large Eddy Simulation, incorporating a one-equation eddy viscosity model to address sub-grid turbulence. The combustion model involved solving the transport equation for a progress variable, governed by flame instabilities and laminar flame speed. Notably, the introduced flame instabilities encompassed Landau-Darrieus instability, Rayleigh-Taylor instability and flame wrinkling factor induced by turbulence. The comparison between predicted results and experimental data revealed an error of less than 50 % for center and rear ignitions. However, this error exceeded 50 % for front ignition. These findings underscore the performance of the CFD model under different ignition conditions, emphasizing the importance of further refinement to enhance predictive accuracy, particularly in scenarios characterized by front ignition.

The Flame Acceleration Simulation (FLACS) software has undergone thorough performance evaluations through extensive comparisons with experimental data (Hisken et al., 2016). Employing the standard Reynolds-Averaged Navier-Stokes (RANS) k-ε model for turbulence resolution and the β model for combustion, the simulation incorporated turbulence induced by fluid venting rather than relying on Rayleigh-Taylor instability to predict external explosions. However, the interaction between the acoustic wave and flame wave was not considered in this model. To address thermal-diffusion effects in quasi-laminar and turbulent stages, the Lewis number was introduced. Real-scale vented hydrogen explosions conducted at the FM Global research campus were simulated, revealing that predicted overpressure and flame speed are larger than the experimental results. Vyazmina and Jallais (2016) utilized the CFD code FLACS v10.4, simulating turbulent flame velocity using Bray's correlation. The flame speed was reduced by a factor beta due to the thickening of the flame front to 3–5 mesh cells. Simulations of vented hydrogen explosions by Daubech et al. (2013), Kuznetsov et al. (2015), and Bauwens et al. (2012a) demonstrated good agreement with experimental data for $K_v < 10$, while discrepancies emerged for large vent coefficient $K_v > 10$, particularly at low hydrogen concentrations. Numerical study conducted by Lakshmipathy et al. (2019), two versions of FLACS v10.7r2, commercial and in-house, were employed to predict real-scale vented hydrogen explosions performed by Skjold et al. (2019). The simulations utilized RANS two equations k-ε and ks-kl turbulence models in FLACS v10.7r2 and FLACS-beta, respectively. The combustion models employed were the Bray model and Bradley model in FLACS v10.7r2 and FLACS-beta, respectively (Bradley et al., 2013; Bray, 1990). Comparative results revealed that predicted overpressure histories by FLACS-beta exhibited better agreement with experimental data than those by FLACS v10.7r2 (Bradley et al., 2013).

Ugarte et al. (2016) established a Computational Fluid Dynamics (CFD) platform grounded in fundamental conservation equations, incorporating considerations for container shape, flame instabilities, and external explosions. To evaluate the model's performance, experimental data from Kumar (2006) and Bauwens et al. (2012a) were employed. The findings of the study indicated that the numerical simulation tended to overpredict the maximum overpressure for rear ignition. However, the predicted results demonstrated good agreement with experimental data for center ignition. This discrepancy underscores the sensitivity of the CFD model's predictive accuracy to specific ignition conditions, emphasizing the need for further refinement and validation under various scenarios to enhance its overall reliability.

Tolias et al. (2018) conducted simulations of vented hydrogen explosions at the FM Global research campus (Bauwens et al., 2011) using four Computational Fluid Dynamics (CFD) codes: FLACS, CFX, FLUENT, and ADREA-HF. The turbulent and combustion models employed in each code are summarized in Table 1. The numerical simulation results revealed that the predicted maximum overpressures by ADREA-HF, FLUENT, and CFX are closely in accordance with experimental data, while FLACS exhibited an overestimation by a factor of 60 %. This discrepancy was attributed to the superior combustion model employed by the former three codes, with the turbulent model having minimal impact on the simulated results. Despite the utilization of the Large Eddy Simulation (LES) turbulence model in ADREA-HF and FLUENT, and the standard two-equation k-ε model in FLACS and CFX, the better performance of the former two codes was attributed to the more suitable combustion model employed, with the turbulence model exerting minimal influence on the simulation results (Tolias et al., 2014, 2017). In terms of flame speed histories, qualitatively accurate simulations were achieved across all codes.

The numerical study of real-scale vented hydrogen explosions, specifically those conducted by FM Global, with center and rear ignitions was undertaken by Tolias et al. (2015). The study focused on examining overpressure histories and flame evolution for 18 % hydrogen-air mixtures. The premixed combustion model employed was based on the turbulent flame speed concept, utilizing Yakhot's equation. Additionally, factors contributing to turbulence generation were incorporated into the model, encompassing the flame front, preferential diffusion, the fractal structure of the flame front, and Rayleigh-Taylor instability. The inclusion of these elements aimed to provide a comprehensive understanding of the dynamics and influencing factors governing vented hydrogen explosions in real-scale containers.

$$S_t = \Xi_k\cdot\Xi_{lp}\cdot\Xi_f\cdot\Xi_{RT}\cdot S_L\cdot\exp\left(\frac{u'}{S_t}\right)^2 \quad (1)$$

The factor account for Rayleigh-Taylor instability $\Xi_{RT} = 1.0$ and $\Xi_{RT} = 1.9$ was tested, simulation results agree well with the experimental data concerning overpressure histories and flame behavior only for $\Xi_{RT} = 1.9$.

Tolias and Venetsanos (2018) conducted an assessment of two combustion models grounded in Yakhot's equation against the KIT vented hydrogen explosion experiment (Kuznetsov et al., 2015). Additionally, a novel model based on Schmid's equation was developed, with consideration given to turbulence induced by the flame front. The predicted results of overpressure-time curves and flame evolution demonstrated improved agreement with the experimental data when compared to the existing models. Notably, flame acceleration within the vessel was found to be predominantly influenced by flame front instabilities, while external explosion dynamics were significantly affected by turbulence.

Madhav Rao Vendra and Wen (2019) developed an in-house Computational Fluid Dynamics (CFD) code, HyFOAM, based on the open-source library OpenFOAM. The turbulence model employed Large Eddy Simulation, with sub-grid turbulence resolved using a one-equation eddy viscosity model. The combustion model incorporated a flame wrinkling model, encompassing the effects of Landau-Darrieus (L-D) instabilities, Rayleigh-Taylor (R-T) instabilities, and thermal-diffusion instabilities. Furthermore, the solver considered the coupling between the fluid and structure. The simulation results demonstrated good accordance with experimental data conducted by Skjold et al. (2019), indicating the efficacy of the developed CFD code in capturing the dynamics of vented hydrogen explosions.

In the comprehensive literature review on numerical studies of vented hydrogen explosions, previous research has led to the development of various codes, with their performance evaluated against specific experiments by comparing internal overpressure histories and typical flame behavior. While some studies have successfully predicted maximum internal overpressure in certain cases and the effects of hydrogen concentration, vent area, vent burst pressure, and blockage ratio were experimentally studied (Chen et al., 2020; Li et al., 2019; Rui et al., 2024; Wang et al., 2022; Xu et al., 2022; Zhang et al., 2022), the mechanism of external explosions remains largely unexplored. This gap arises from limited attention to overpressure-time curves, which are often compared only within specific experiments of fuel-lean hydrogen-air mixtures. Furthermore, the validation of CFD software for different ignition locations, hydrogen concentrations, and container sizes has been scarce. Due to the enhanced capacity of numerical simulations to furnish comprehensive insights into the flow field compared to experiments, they prove invaluable in elucidating the mechanisms underlying external explosions. In the current study, a turbulent combustion model based on Schmidt correlation was developed within the CFD code GASFLOW-MPI. Initially, GASFLOW-MPI was validated against experimental data. The study then reveals the mechanisms governing pressure rise within the vessel and the generation of overpressure peaks induced by external explosion. Subsequently, the effects of turbulence models on overpressure histories were investigated, along with examination of heat transfer on overpressure histories. Moreover, considering the significant engineering implications of vented hydrogen explosions, the research assesses the performance of the numerical model across a spectrum of fuel-lean to fuel-rich hydrogen-air mixtures and various ignition locations, drawing comparisons with experimental data. The model's predictive capabilities for medium-scale vented hydrogen explosions are also assessed. This comprehensive approach aims to contribute valuable insights into the complex dynamics of vented hydrogen explosions and enhance the predictive accuracy of numerical models, which would provide a more accurate numerical tool for predicting the overpressure during vented hydrogen explosions.

2. Numerical models

Mass conservation equation (Xiao et al., 2017c)

The mass conservation equation is given by

$$\frac{\partial}{\partial t}\int_V \rho dV = \oint_S \rho(\mathbf{b} \quad \mathbf{u})\cdot \mathbf{A} dS + \int_V S_\rho dV \tag{2}$$

where ρ is the mixture density or the sum of the macroscopic densities for each individual species, $\mathbf{u}$ is the mass-average velocity vector, where $\mathbf{b}$ is the velocity of the contour surface S', The term $\mathbf{b} - \mathbf{u}$ is the relative velocity between the control surface and the fluid. $\boldsymbol{A}$ and dS are the outward normal fractional area vector and differential area, respectively, of material surface S bounding V. S_ρ is the mass source or sink term.

The mixture-momentum transport conservation equation is given by

$$\frac{d}{dt}\int_V \rho \mathbf{u} dV = \oint_S \rho \mathbf{u}(\mathbf{b} \quad \mathbf{u})\cdot \mathbf{A} dS \quad \oint_S p d\mathbf{S} + \int_V \rho \mathbf{g} dV \quad \oint_S (\tau\cdot\mathbf{A}) dS \quad \oint_S (\mathbf{D}_d\cdot\mathbf{A}) dS + \int_V \mathbf{S}_m dV \tag{3}$$

where p is the pressure, $\boldsymbol{\tau}$ is the viscous stress tensor, g is the gravitational vector, $\boldsymbol{D}_d$ is the internal structure drag tensor, and $\boldsymbol{S}_m$ is any momentum sources. The right-side integrals represent, respectively, the flux of momentum through the control surface, the sum of pressure gradient, gravity, and viscous forces on the control volume, fluid drag forces acting on structural surfaces; and any additional momentum sources.

The equation of change for the total energy is

$$\frac{d}{dt}\int_V \rho I dV = \oint_S \rho I(\mathbf{b} \quad \mathbf{u})\cdot \mathbf{A} dS \quad \oint_S p(\mathbf{u}\cdot\mathbf{A}) dS \quad \int_V \left[\frac{p}{V}\frac{\partial V_{h_2o}}{\partial t}\right] dV \quad \oint_S (\mathbf{q}\cdot\mathbf{A}) dS + \int_V S_I dV \tag{4}$$

where I is the mixture specific internal energy, and S_I is the energy source or sink term per unit volume and time. The energy flux vector $\mathbf{q}$ is given by

$$\mathbf{q}\cdot\mathbf{A} = \left\{ \begin{array}{l} A_x\left[\phi_x \dfrac{\partial T}{\partial x} \quad \sum\limits_\alpha h_\alpha J_{x,\alpha}\right], \\ A_y\left[\phi_y \dfrac{\partial T}{\partial y} \quad \sum\limits_\alpha h_\alpha J_{y,\alpha}\right], \\ A_z\left[\phi_z \dfrac{\partial T}{\partial z} \quad \sum\limits_\alpha h_\alpha J_{z,\alpha}\right] \end{array} \right\} \tag{5}$$

where ϕ_i is the molecular conductivity and h is the enthalpy for species α.

The transport equation for individual species is given by

$$\frac{\partial}{\partial t}\int_V \rho_\alpha dV = \oint_S \rho_\alpha(\mathbf{b} \quad \mathbf{u})\cdot \mathbf{A} dS \quad \oint_S (\mathbf{J}_\alpha\cdot\mathbf{A}) dS + \int_V S_{\rho,\alpha} dV \tag{6}$$

where α denotes the gas species, ρ_α is the mass per unit volume (macroscopic density), $J_\alpha \cdot A$ is the mass diffusion flux vector with Cartesian geometry components $\left(A_x J_{x,\alpha}, A_y J_{y,\alpha}, A_z J_{z,\alpha}\right)$, and the source or sink term, $S_{\rho,\alpha}$, represents the species mass created or destroyed by chemical reactions and two-phase change dynamics of the liquid and vapor water components.

In current study, four turbulence models, Reynolds-averaged (RANS) turbulence model k-ε (Xiao et al., 2018), shear stress transport SST κ-ω model(Xiao et al., 2016a), detached eddy simulation DES turbulence model (Zhang et al., 2018a), and Large Eddy Simulation (LES) turbulence model (Zhang et al., 2018b) were tested.

3. Combustion model

In the computational fluid dynamics (CFD) software GASFLOW-MPI, a combustion model relying on the progress variable was previously established(Xiao et al., 2016b). In the present investigation, an advanced multi-phenomena combustion model, grounded on the Schmidt correlation, was developed (Schmid et al., 1998). It incorporates additional factors influencing flame acceleration and wrinkling. Specifically, the model considers flame wrinkling factors induced

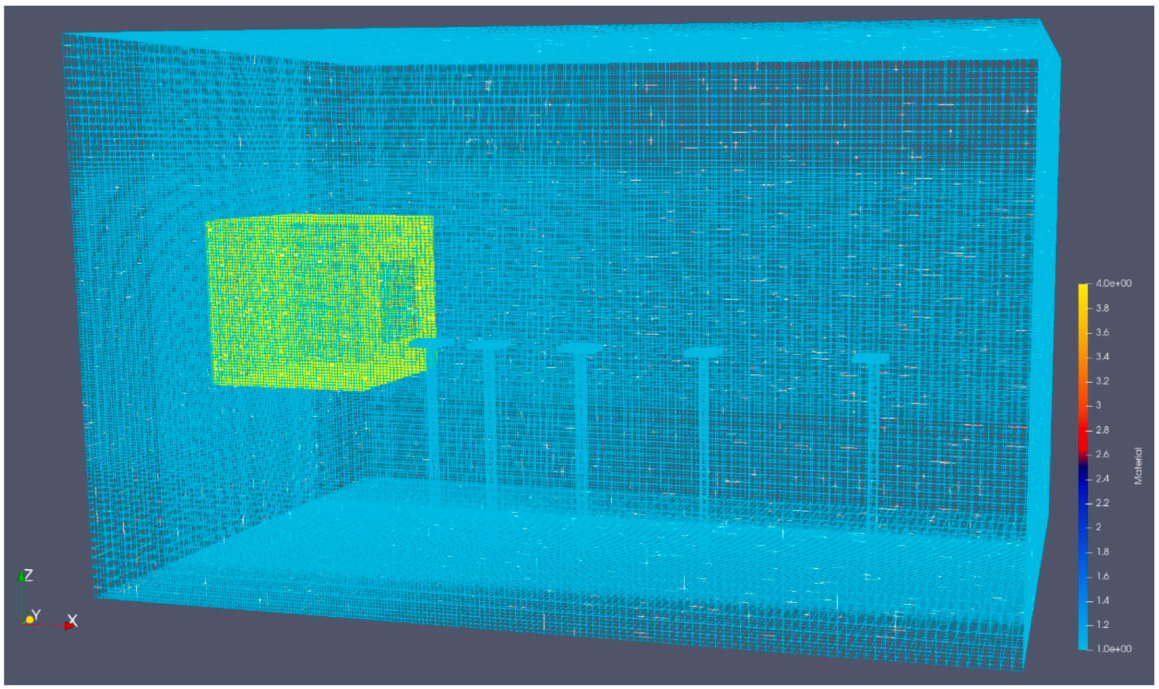

Fig. 1. Three-dimensional grid used in the current study.

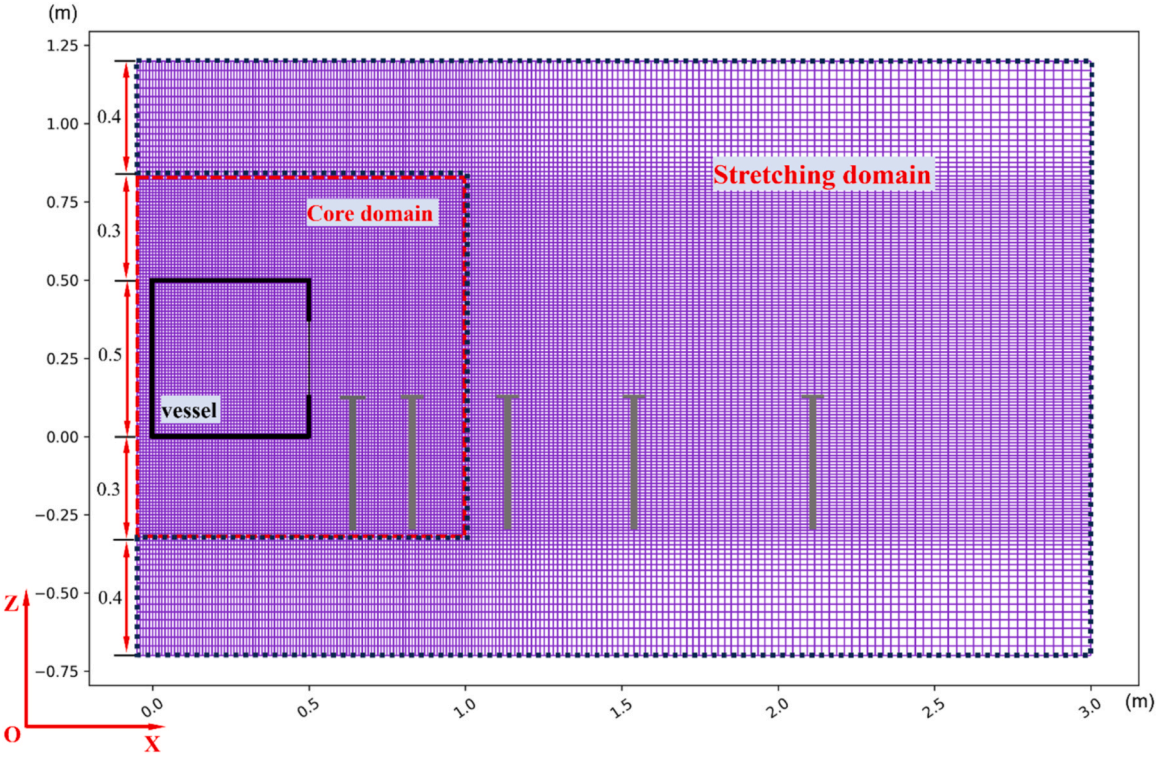

Fig. 2. Schematic of the grid used in the current study.

by two intrinsic instabilities: Thermal-Diffusive instabilities and Landau-Darrieus instabilities (Bauwens et al., 2019; Landau, 1944; Lewis and von Elbe, 1987). Thermal-Diffusive instabilities arise from the imbalance of heat and species diffusion, while Landau-Darrieus instabilities result from thermal expansion across the flame surface. Consequently, the effective turbulent flame model is expressed as follows, encompassing these intricate phenomena.

$$S_{eff} = F_{plp}\Xi_{lp}\Xi_{turb}S_t \tag{7}$$

Where F_{lpl} is pressure correction factor for Ξ_{lp}, Ξ_{lp} is flame wrinkling factor responsible for the Thermal-Diffusive instabilities and Landau-Darriues instabilities coupled with flamelet curvature. Ξ_{turb} is factor for turbulence generated by the flame front itself.

Pressure correction factor F_{lpl} is calculated as follows.

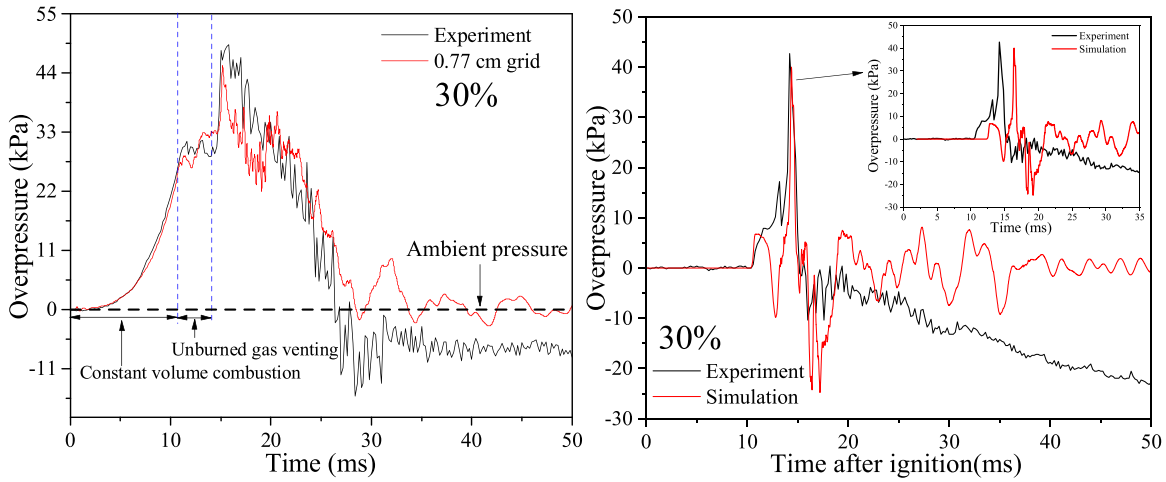

Fig. 3. Comparison of experimental data (Rui et al. 2021) and simulation results for internal (left) and external (right) overpressure time profiles of 30 % hydrogen-air mixtures.

$$F_{plp} = \frac{\Xi_{lp}}{\Xi_{lp,0}} = \left(\frac{P}{P_0}\right)^{0.14} \left(P_0 = 1bar\right) \tag{8}$$

Corrected leading point coefficient coupled with flamelet curvature Ξ_{lp} can be expressed as follows.

$$\Xi_{lp} = F_{plp}\Xi_{lp,0} = \begin{cases} \left(\frac{P}{P_0}\right)^{0.14} \left[1 + \frac{\left(\Xi_{lp}^{\max} \quad 1\right)\cdot 2R}{R_0}\right], R < \frac{R_0}{2} \\ \left(\frac{P}{P_0}\right)^{0.14} \Xi_{lp}^{\max}, R \geq \frac{R_0}{2} \end{cases} \tag{9}$$

Where R is the distance from the ignition point to the flame front, R_0 is the critical radius which is about 1.0–1.2 m for near-stoichiometric hydrogen/sir mixtures. Maximum leading point coefficient $\Xi_{lp}^{\max}$ can be expressed as follows.

$$\Xi_{lp}^{\max} = \max\left(Le_{eff}^{-0.8}, 1\right) \tag{10}$$

Flame wrinkling factor Ξ_{turb} due to self-induced turbulence can be expressed as:

$$\Xi_{turb} = 1 + \left(\psi\cdot\Xi_{turb}^{\max} \quad 1\right)\cdot\left[1 \quad e^{-(R/R_0)}\right] \tag{11}$$

Model constant ψ is close to $\psi = 0.5$ for near-stoichiometric mixtures, and it grows to maximum value $\psi = 1$ for lean hydrogen/air mixtures. Maximum flame wrinkling factor $\Xi_{turb}^{\max}$ due to self-induced turbulence is calculated as follows.

$$\Xi_{turb}^{\max} = \frac{(\sigma \quad 1)}{\sqrt{3}} \tag{12}$$

Expansion coefficient or ratio σ of densities of the unburned mixture and the combustion products.

$$\sigma = \quad 3.25\Phi^2 + 9.05\Phi + 1.4 \tag{13}$$

In current study, turbulent flame model based on Schmidt correlation was utilized. Schmidt correlation is as follows.

$$S_T = S_L + u'\left(\frac{Da^2}{1 + Da^2}\right)^{0.25} \tag{14}$$

Damkoehler number Da is defined as the ratio of the turbulent integral time scale to the chemical time scale.

$$Da = \frac{\tau_t}{\tau_c} = \frac{l_t S_L^2}{\alpha u_t'} \tag{15}$$

$$l_t = C_D\frac{\left(u_t'\right)^3}{\varepsilon} \tag{16}$$

Where C_D is the turbulent length scale constant, ε is the turbulent dissipation rate, α is the thermal diffusivity.

4. Heat transfer model

4.1. Convection heat transfer

Heat transfer resulting from convection between the high-temperature combustion product and the walls of the explosion vessel can be mathematically expressed as follows (Xiao et al., 2016a):

$$S_{I,\text{conv}} = h_s A_s\left(T_s \quad T\right) \tag{17}$$

The convective heat transfer coefficient, denoted as h_s, between the gas mixture and the internal vessel surfaces, is expressed in units of W/(m^2·K). Where A_s represents the total area of the internal vessel surface in square meters, T_s is the temperature of the internal vessel surface, and T is the temperature of the combustion product. The calculation of the convective heat transfer coefficient h_s is determined by the following expression (Bird et al., 1960).

$$h_s = \frac{\tau_s}{|u_c|}C_p\cdot\mathrm{Pr}^{-2/3} \tag{18}$$

Where τ_s is the wall shear stress, u_c is the average speed of the control volume center, C_p is molar heat capacity at constant pressure, $J/(g\cdot K)$. Pr is Prandtl number.

4.2. Thermal radiation model

In the current study, the impact of thermal radiation was investigated due to the generation of high-temperature combustion products. Given that the thermal radiations from gas mixture species H_2, N_2, and O_2 were considered negligible, the dominant contribution to thermal radiation stems from water vapor. Therefore, the influence of water vapor was solely considered in the thermal radiation model (David, 1942; Hadjipanayis et al., 2015). The thermal radiation transport equation, governing the gray gas used in GASFLOW-MPI, is expressed as follows (Chandrasekhar, 1960; Siegel and Howell, 1992; Sparrow and Cess, 1978).

$$\frac{1}{c}\frac{\partial E(r,\Omega,t)}{\partial t} + l_i\frac{\partial E(r,\Omega,t)}{\partial x_i} = \quad \zeta E\left(r,\Omega,t\right) + \frac{\zeta\sigma T^4}{\pi} \tag{19}$$

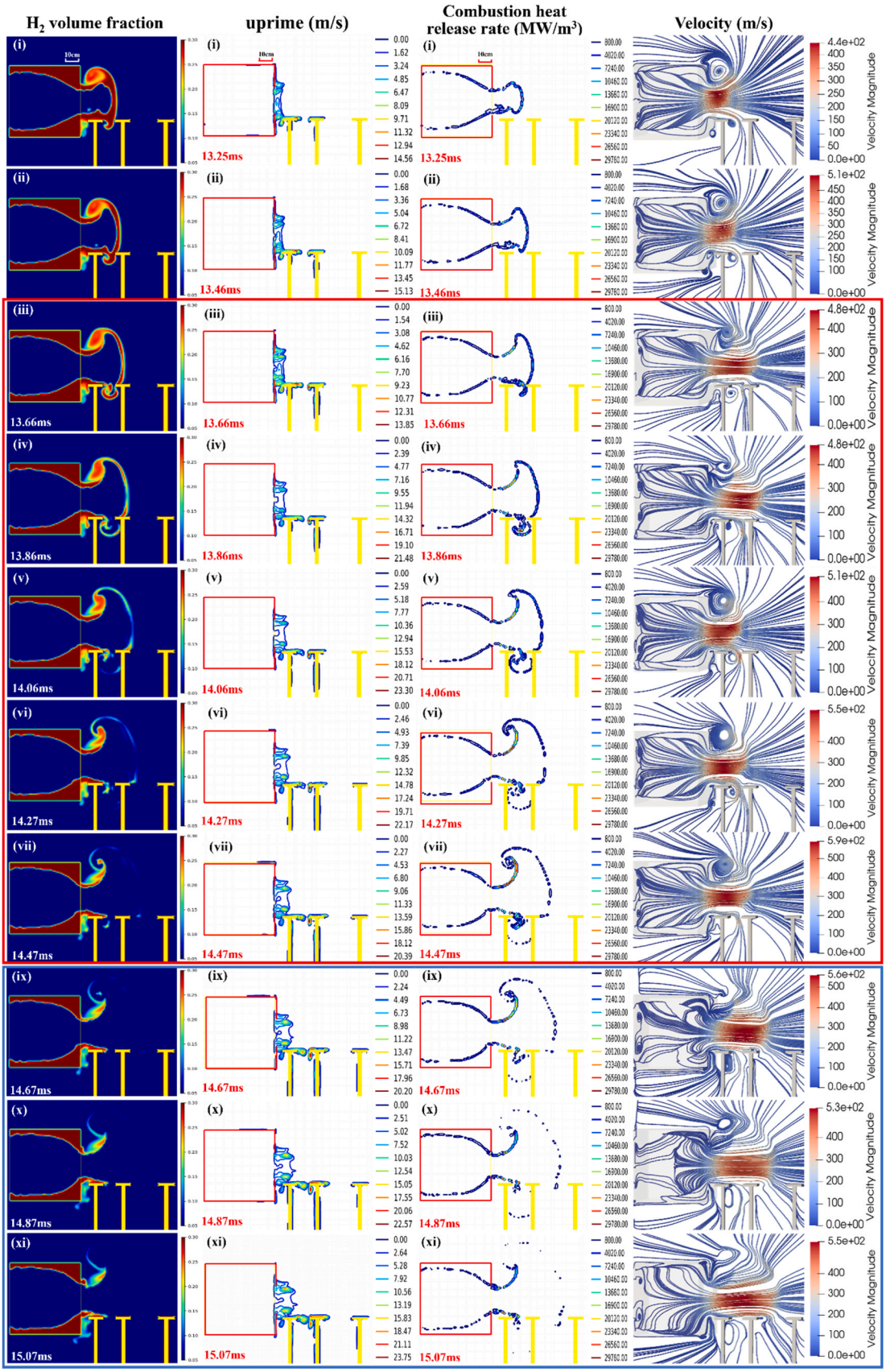

Fig. 4. Hydrogen volume fraction, turbulence intensity (u' contours), combustion heat release rate, and fluid velocity at the central XZ plane.

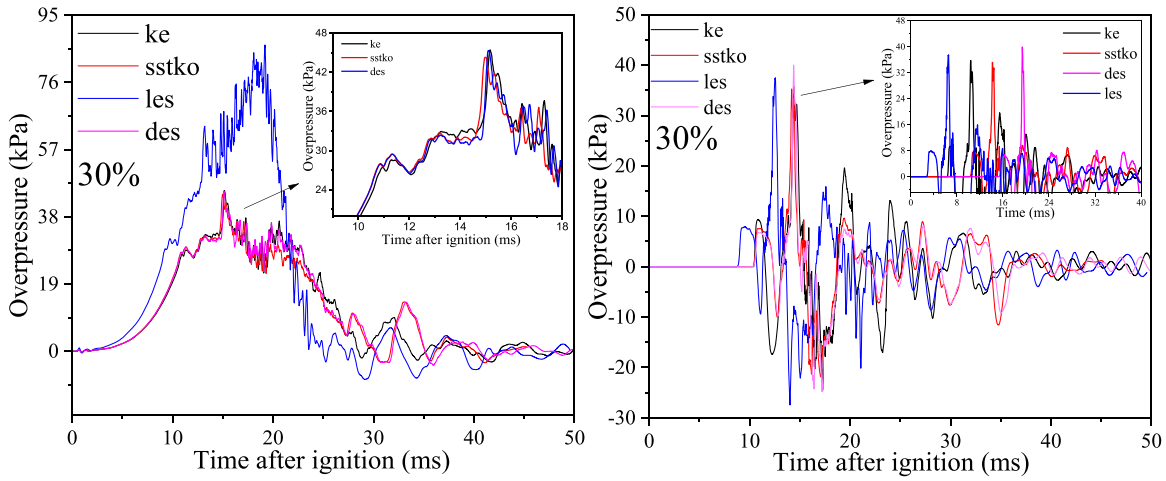

Fig. 5. Internal (left) and external (right) overpressure-time curves for different turbulence models.

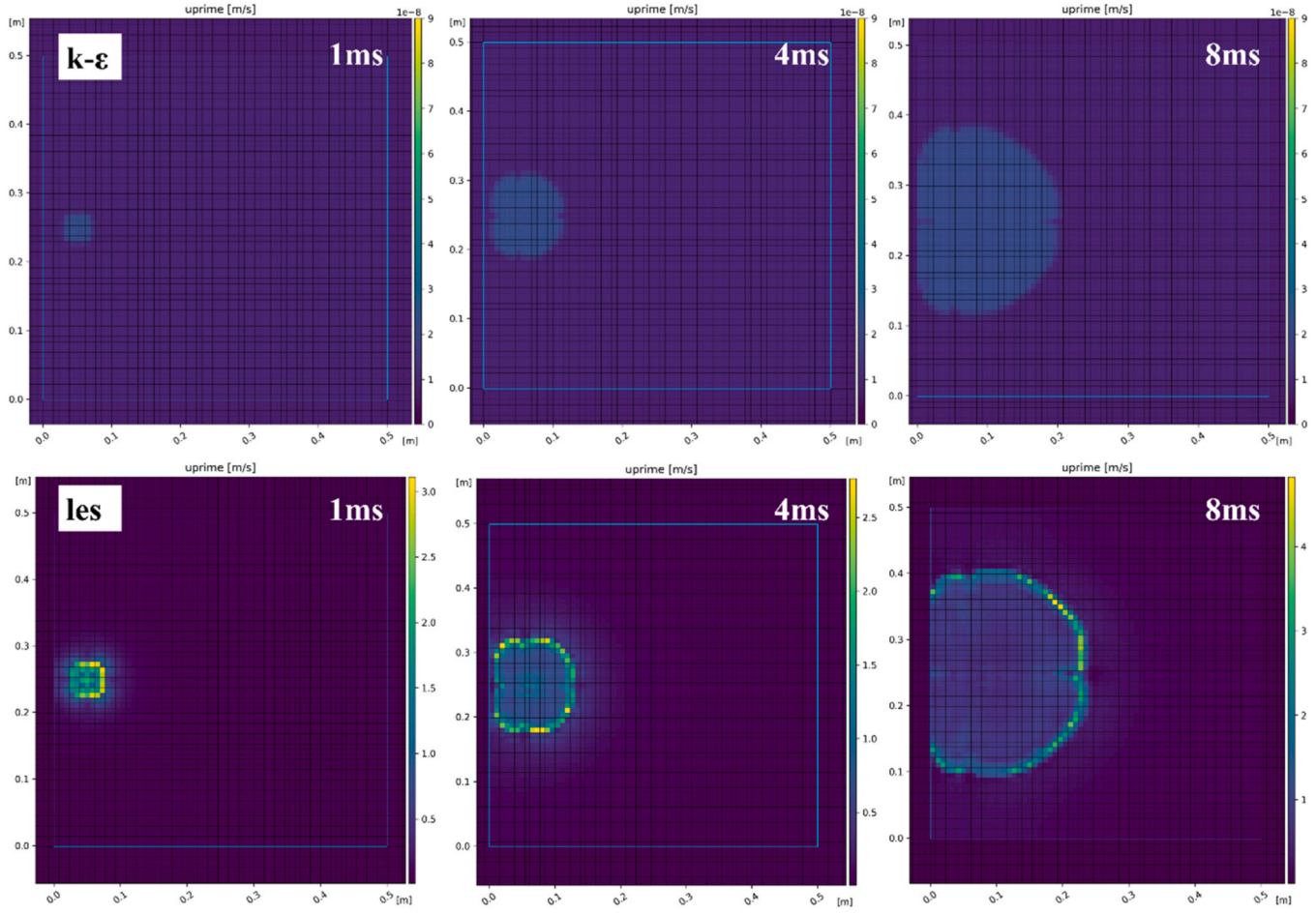

Fig. 6. The change of uprime (u') inside the vessel with the time for different turbulence models.

Where c is the speed of light, specific radiation intensity $E(r, \Omega, t)$is related to the position vector $\boldsymbol{r}$, directional vector Ω, and the time t. $\zeta$is the absorption coefficient, σ is the Stefan-Boltzmannn constant, and T is the temperature of the gas.

4.3. Steam condensation and evaporation

In the context of hydrogen explosions, a significant amount of high-temperature water vapor is generated. Consequently, heat transfer due to steam condensation was considered in the current study(Xiao et al., 2018). The heat flux resulting from steam condensation or evaporation on the vessel wall surface can be mathematically expressed as follows (Xiao et al., 2016a).

$$q_{s,cond,vap} = \max\begin{cases} h_d A_s\left(\rho_{H_2O} \quad \rho_{s,saturation}\right) I_{H_2O}(T_s) \\ h_d A_s\left(\rho_{H_2O} \quad \rho_{s,saturation}\right) I_{H_2O}(T) \end{cases} \tag{20}$$

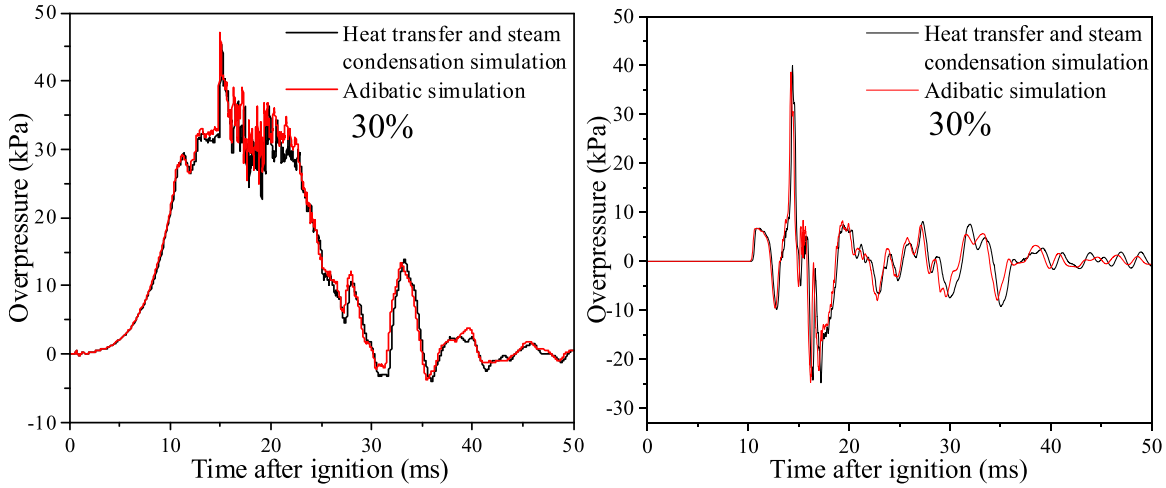

Fig. 7. Internal (left) and external (right) overpressure-time curves for adiabatic simulation and numerical simulation considering heat transfer and condensation.

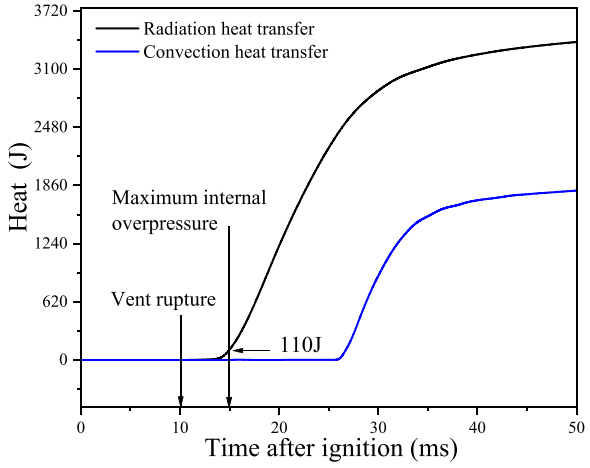

Fig. 8. Heat transfer due to thermal radiation and convection.

Where $I_{H_2O}(T_s)$ and $I_{H_2O}(T)$is specific internal energy of the liquid water film and water vapor, respectively, h_s is the mass transfer coefficient, $\rho_{H_2O}$is the density of water vapor. The saturation density $\rho_{s,saturation}$is a function of saturation pressure $P_{s,sat}(Ts)$ and the structural surface temperature T_s and expressed as

$$\rho_{s,sat}\left[T_s, P_{s,sat}(T_s)\right] = \frac{P_{s,sat}(T_s)}{R_{H_2O}\cdot T_s} \tag{21}$$

Where R is universal gas constant, the mass transfer coefficient, h_d, is derived from the heat transfer coefficient, h_s, as (Bird et al. 1960)

$$h_d = \frac{h_s}{\rho C_p}\frac{Sc^{-2/3}}{\mathrm{Pr}^{-2/3}} \tag{22}$$

Where Sc is the Schmidt number.

5. Numerical simulation setup

5.1. Geometry model

In accordance with the experimental study on vented hydrogen explosions referenced, a three-dimensional geometry was established in GASFLOW-MPI (Rui et al., 2021), as shown in Fig. 1. The vessel walls were constructed with stainless steel material. The setup included a vent with a size of 0.25 m × 0.25 m and a rupture pressure of approximately 22 kPa, matching the parameters of the experiment. The side length of the vessel was 0.5 m. The ignition point, located at the centerline between the back wall and the vent, was positioned at distances of 0.05 m and 0.25 m from the back wall, corresponding to rear ignition and center ignition, respectively. Monitoring points were designated with

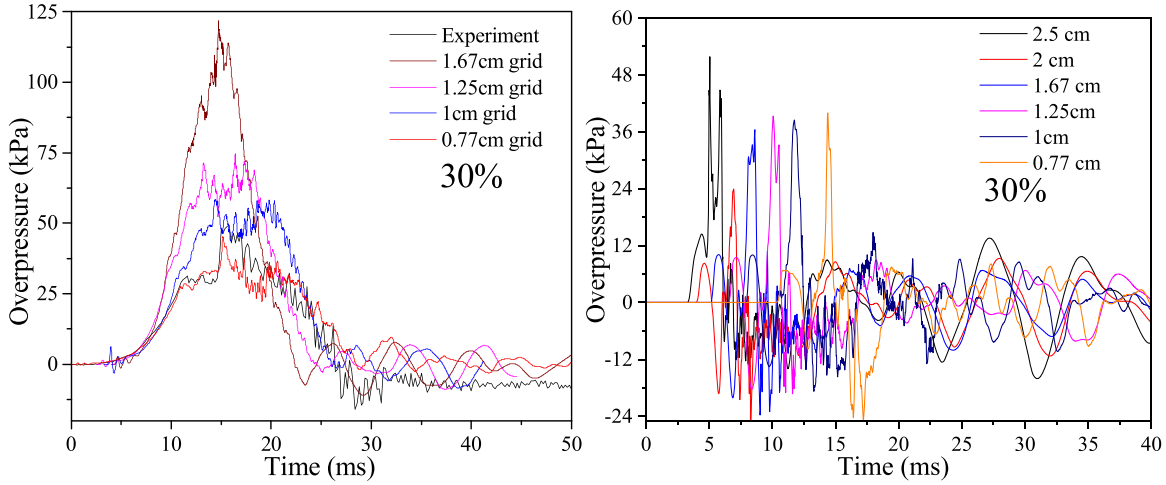

Fig. 9. Internal (left) and external (right) overpressure time curves predicted with different grid sizes for 30 % hydrogen-air mixtures

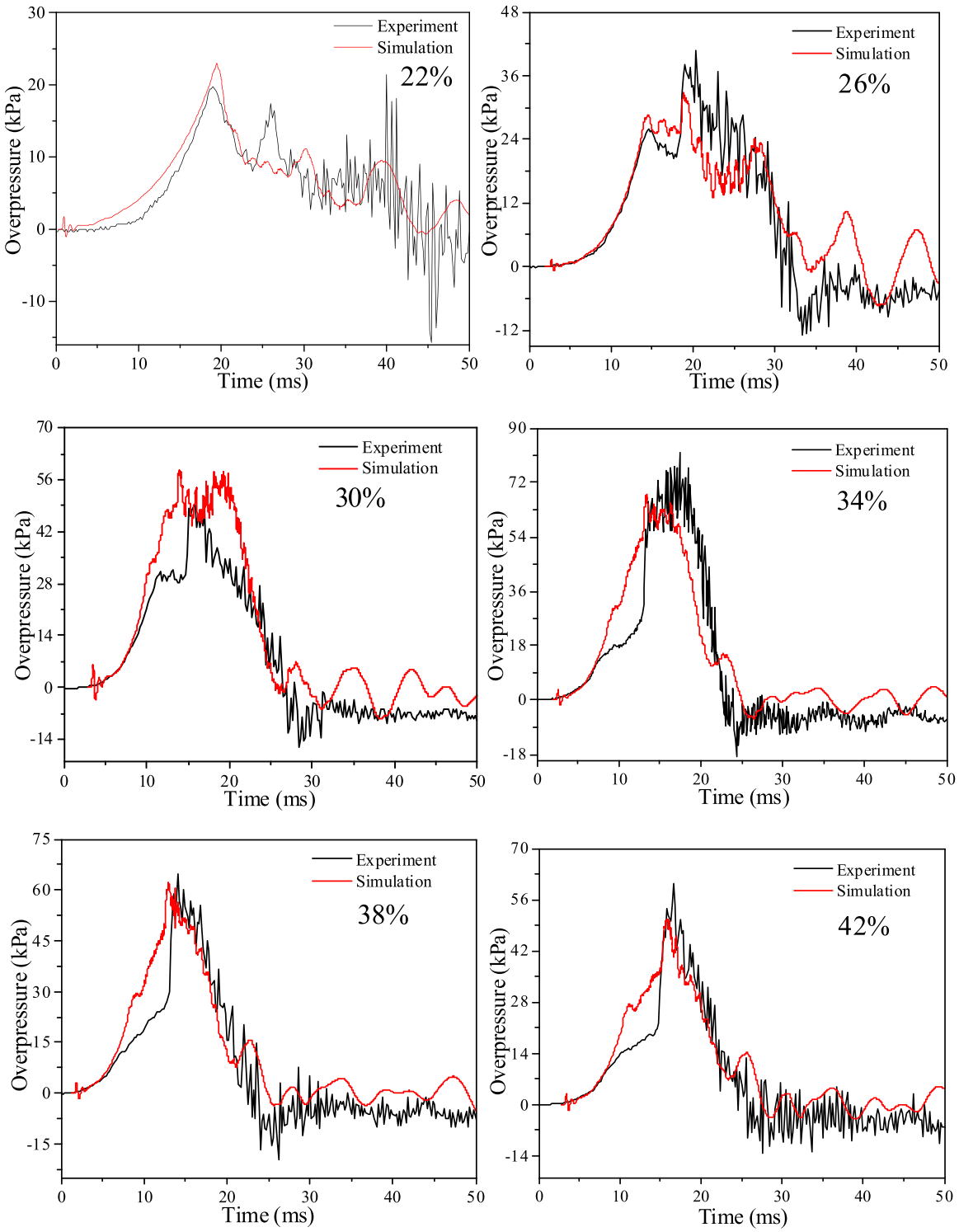

Fig. 10. Comparison between the experimental data(Rui et al. 2021) and simulation results for rear ignition.

coordinates mirroring those in the experiment. An internal monitoring point was located at the centerline of the internal top wall, 0.05 m away from the back wall. Meanwhile, external monitoring points were aligned with the lower edge of the vent and placed same distances away from it as the experiment. These configurations aim to replicate the experimental conditions and facilitate a comprehensive numerical analysis of vented hydrogen explosions.

5.2. *Initial and boundary conditions*

In the current study, based on the flame images recorded during the experiment, the computational domain was divided into two distinct regions: (1) the core domain where the premixed hydrogen-air mixture reacts, and (2) the stretching domain extending from the core domain to the boundaries. The vent was positioned in the positive direction of the X-axis, and the gravitational direction was defined as the negative Z-axis. A cuboid grid was employed in the core domain, encompassing (1)

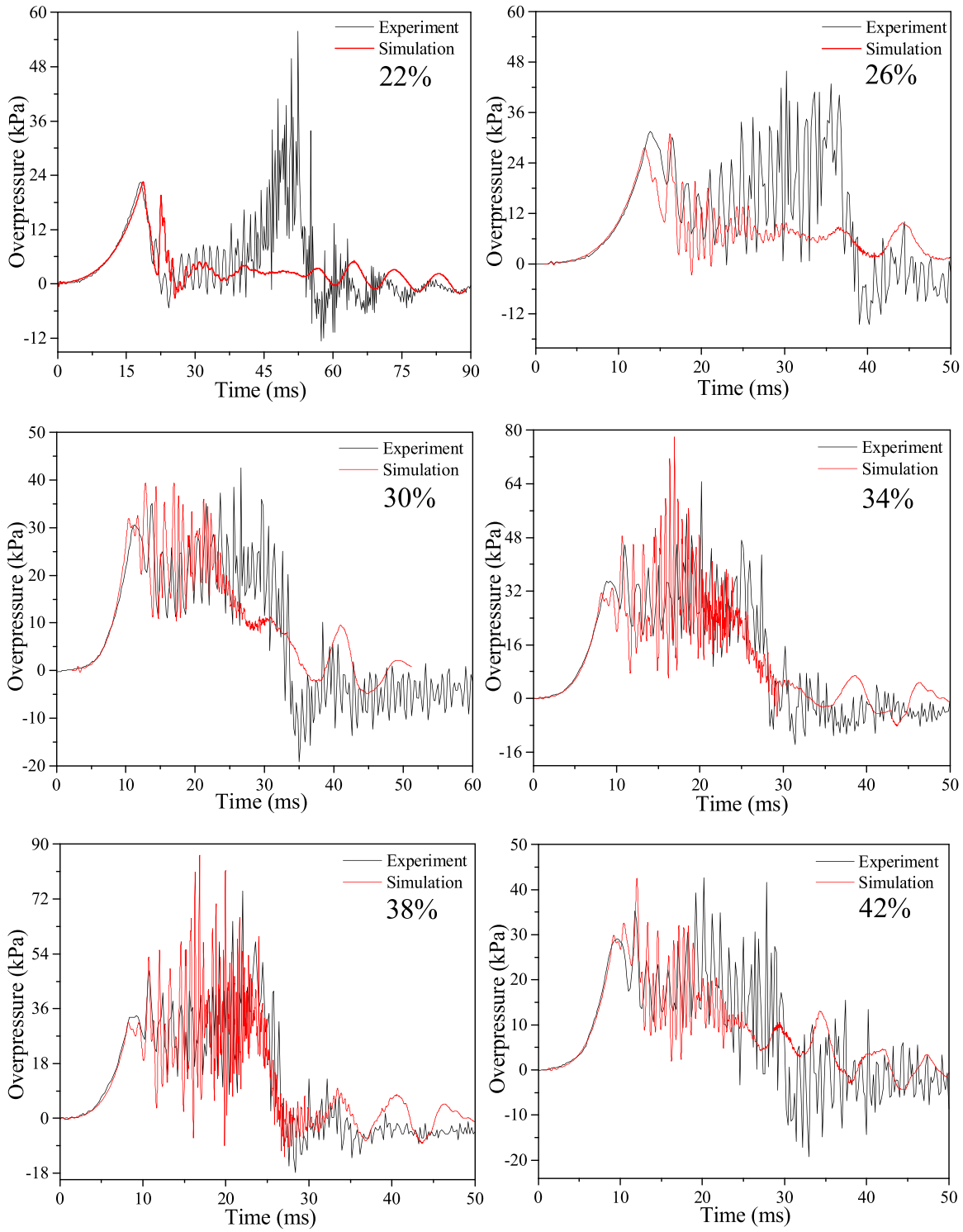

Fig. 11. Comparison between the experimental data (Rui et al. 2021) and simulation results for center ignition.

the entire vessel, (2) the region outside the vessel extending 0.5 m away from the vent, and (3) the regions outside the vessel located 0.3 m away from the top wall, bottom wall, north wall, and south wall, respectively, as depicted in Fig. 2. The initial temperature and pressure were set to 300 K and 101,325 kPa, respectively, mirroring the conditions of the experiment. All boundary conditions were specified as no-slip, contributing to a comprehensive numerical representation of vented hydrogen explosions.

6. Results and discussion

Fig. 3 illustrates the comparison between experimental data and simulation results of internal and external overpressure histories of 30 % hydrogen-air mixtures for rear ignition. In the numerical simulation, a 0.77 cm cuboid grid was utilized in the core domain, resulting in a total of approximately 4, 018, 000 cells. It is evident that the predicted internal and external overpressure-time curves agree well with the experimental data, although the predicted maximum overpressure are

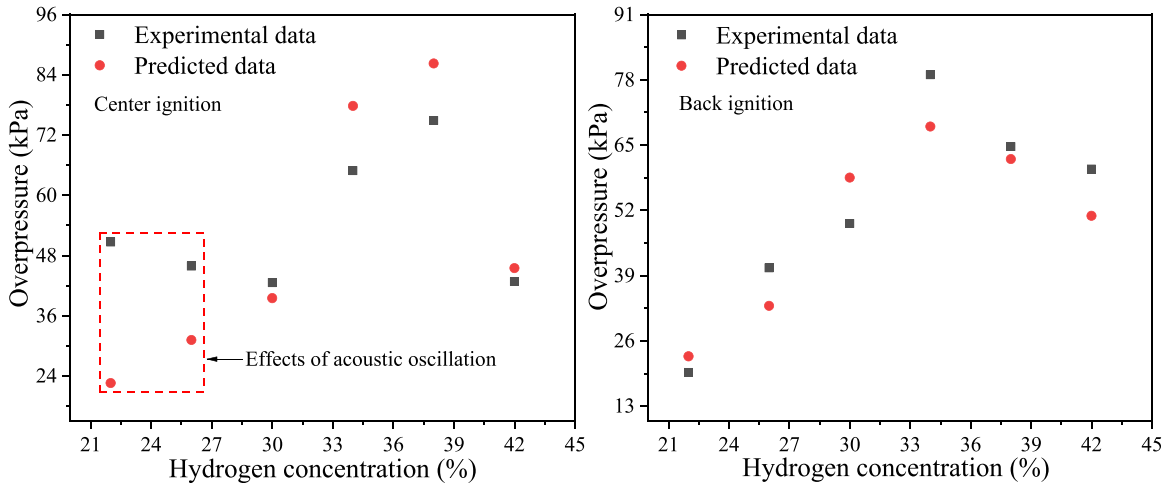

Fig. 12. Comparison of the maximum internal and external overpressure between the experimental data(Rui et al. 2021) and predicted data (left: center ignition, right: rear ignition).

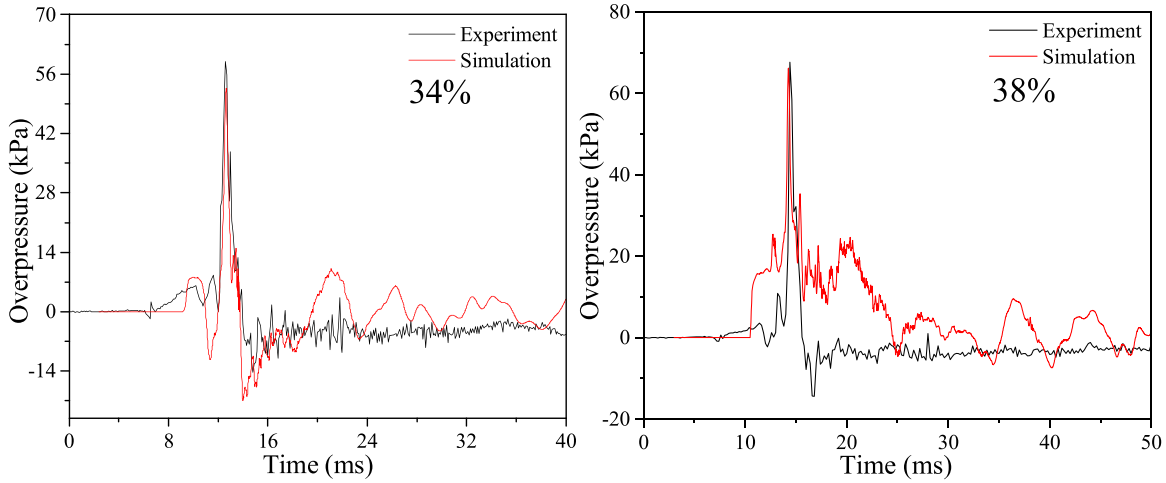

Fig. 13. Comparison between the experimental data(Rui et al. 2021) and simulation results of external overpressure-time curves for rear ignition.

slightly lower than those observed experimentally.

The internal overpressure-time curve can be segmented into three stages: (1) constant volume deflagration, (2) unburned mixture venting, and (3) external explosion. During the constant volume deflagration stage, the overpressure rise rate primarily associated with flame instabilities and laminar flame velocity. In the numerical model, the turbulent flame speed $S_T = S_L + u'\left(\frac{Da^2}{1+Da^2}\right)^{0.25}$ is nearly equal to the laminar flame speed in the initial stage of deflagration. Despite the flame approaching the back wall, the heat transfer from the flame to the vessel walls has a minimal effect on internal overpressure, which will be discussed later

From the numerical simulation results, it can be found that the unburned mixture is expelled from the vessel at t = 11 ms, with the venting rate increasing from 60 m/s to about 200 m/s at t = 12.6 ms. The internal flame front expands, resulting in the overpressure rise due to internal chemical reactions being nearly equivalent to the pressure drop induced by unburned mixture venting. A slight discrepancy in the first overpressure peak between the predicted value and experimental data arises from differences in vent rupture pressure in the experiment. The opening pressure of the vent is subject to some error in the experimental setup.

Fig. 4 presents the evolution of hydrogen volume fraction, turbulence intensity (uprime), combustion heat release rate, and velocity over time. Focusing on the period from t = 13.66 ms to t = 14.47 ms (highlighted in the red box in Fig. 4) corresponding to the formation of the external maximum overpressure peak, it is observed that the flame area and flame propagation velocity experience a rapid increase, transitioning from approximately 480 m/s to about 590 m/s. In addition to the ignition induce by high-speed jet flame, strong turbulence intensity is maintained near the vent and around the rod, and the combustion heat release rate also shows an increase. The maximum external overpressure is generated when the vented unburned mixture is completely consumed.

As a result of the maximum external overpressure occurring at t = 14.47 ms, the internal overpressure experiences a rapid increase from t = 14.67 ms to t = 15.07 ms. The changes in hydrogen volume fraction, turbulence intensity (uprime), combustion heat release rate, and velocity during this period are depicted in the blue box in Fig. 4. It can be found that the combustion heat release rate increases from t = 14.67 ms to t = 14.87 ms. Additionally, the flame venting rate decreases from about 590 m/s at t = 14.47 ms to approximately 530 m/s at t = 14.87 ms. This indicates an increase in the chemical reaction rate concurrent with a decrease in the venting rate, leading to a rapid increase in internal overpressure.

Fig. 5 illustrates the effects of turbulence models on internal and external overpressure-time profiles. It is observed that the internal overpressure-time curves predicted using Reynolds-averaged (RANS)

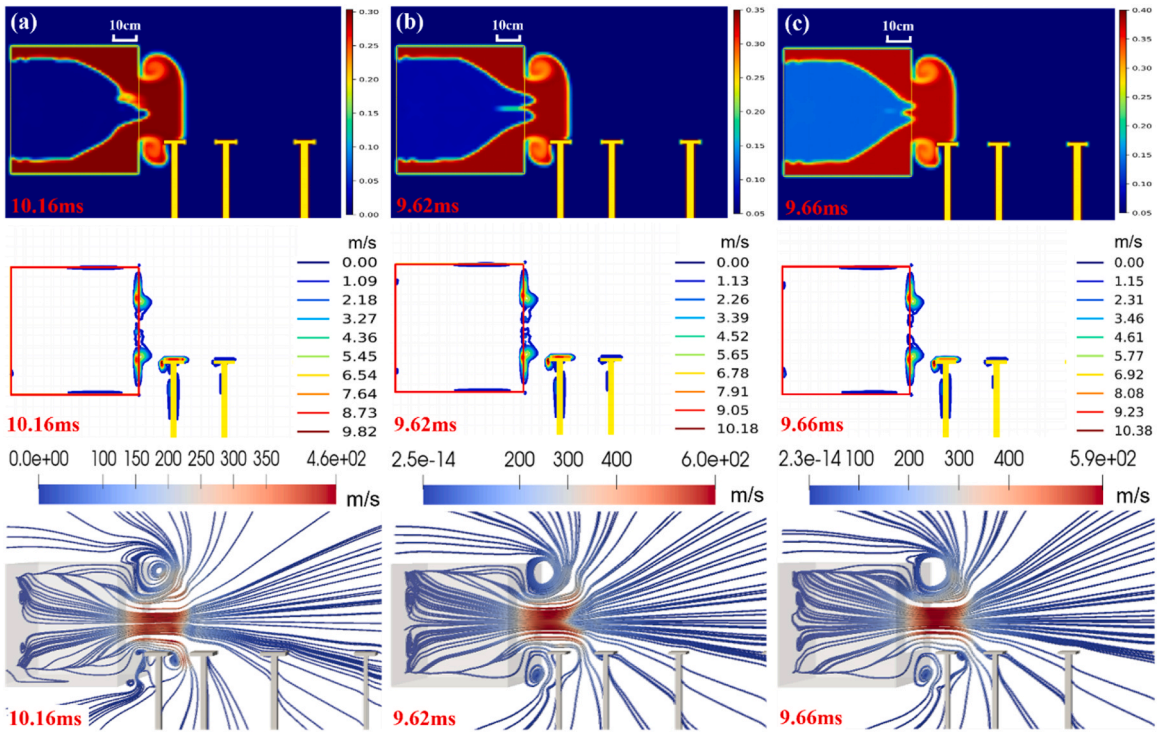

Fig. 14. Turbulence intensity (u' contours), hydrogen volume fraction, and fluid velocity at the central XZ plane for hydrogen-air mixtures with different concentrations (Left: 30 %, center: 34 %, right: 38 %).

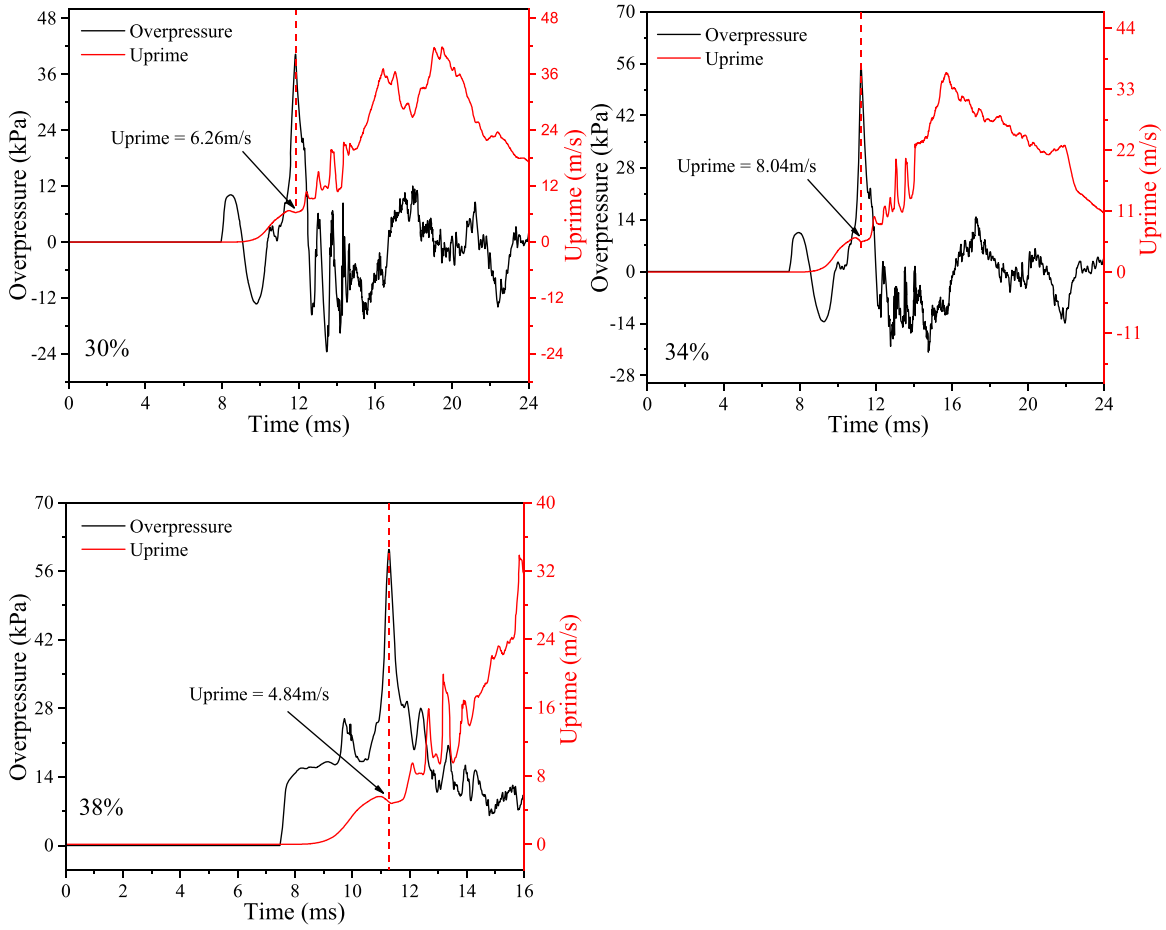

Fig. 15. External overpressure-time curves and turbulence intensity (u')-time profiles for different hydrogen concentrations (Left: 30 %, center: 34 %, right: 38 %).

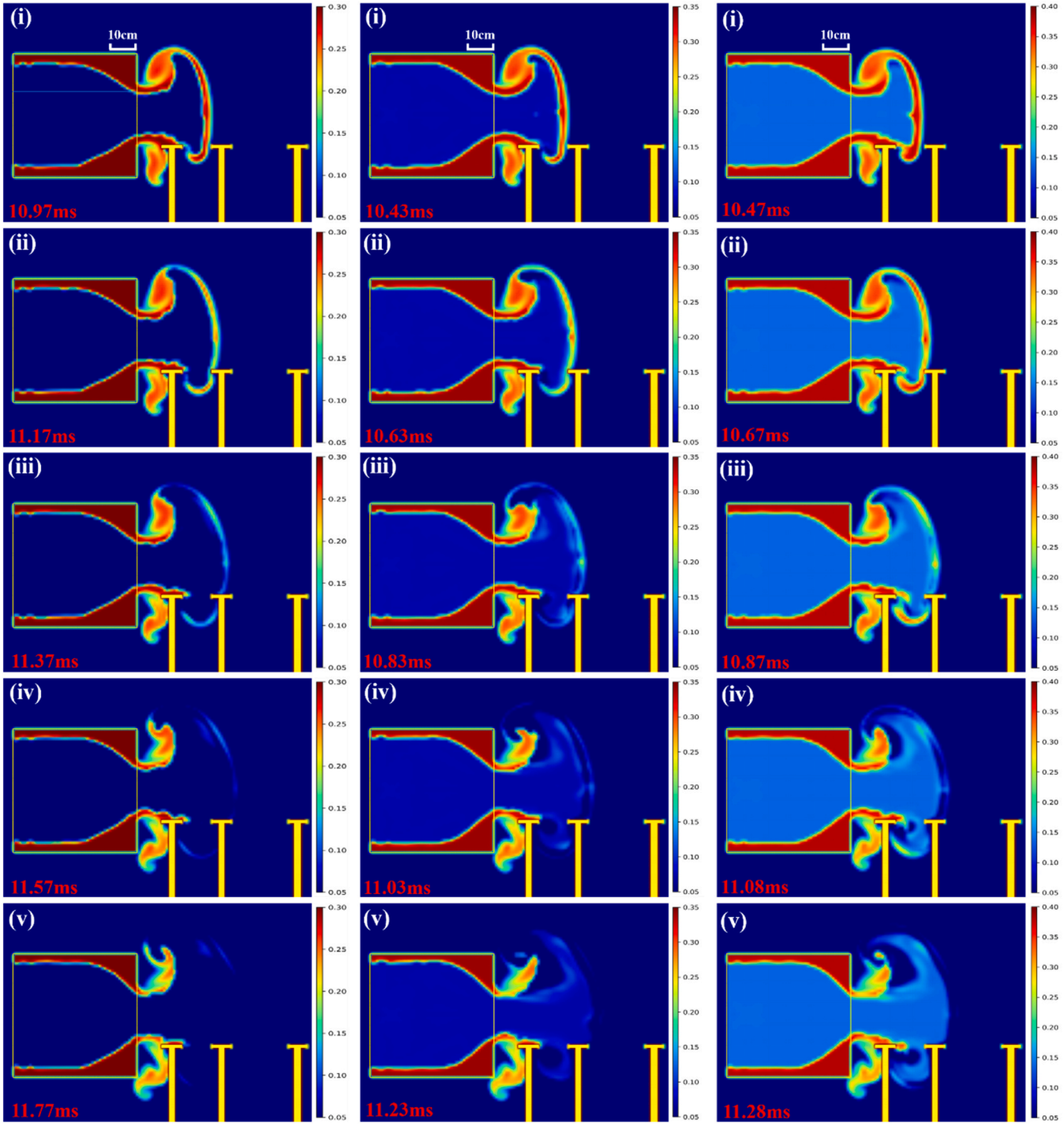

Fig. 16. Hydrogen volume fractions just before the maximum external overpressure for different hydrogen concentrations (left: 30 %, center: 34 %, right: 38 %).

turbulence model k-ε, shear stress transport SST κ-ω model, and detached eddy simulation DES turbulence models exhibit nearly identical trends over time. However, the overpressure predicted using the Large Eddy Simulation (LES) turbulence model is larger than those predicted using k-ε and SST-k-ω turbulence models. This discrepancy arises because the LES model tends to overpredict the turbulence intensity inside the vessel. Particularly in the early stages of deflagration, chemical reactions are dominated by laminar combustion velocity and intrinsic flame instabilities rather than turbulent combustion, as discussed previously. Fig. 6 displays the variation of turbulence intensity (uprime u′) inside the vessel calculated using k-ε and LES turbulence models. The turbulence intensity calculated using the LES model is approximately 2–4 m/s, significantly exceeding that calculated using the k-ε turbulence model. The turbulent flame model $S_T = S_L + u'\left(\frac{Da^2}{1+Da^2}\right)^{0.25}$ employed in the current study considers that the chemical reaction in the initial stages of deflagration is dominated by laminar flame velocity. However, the LES turbulence model assumes an initial turbulence intensity of uprime = 0.026 m/s, leading to an overprediction of turbulence intensity. Consequently, the LES model overpredicts the first peak overpressure, disrupting the balance between pressure rise from internal chemical reactions and pressure drop from

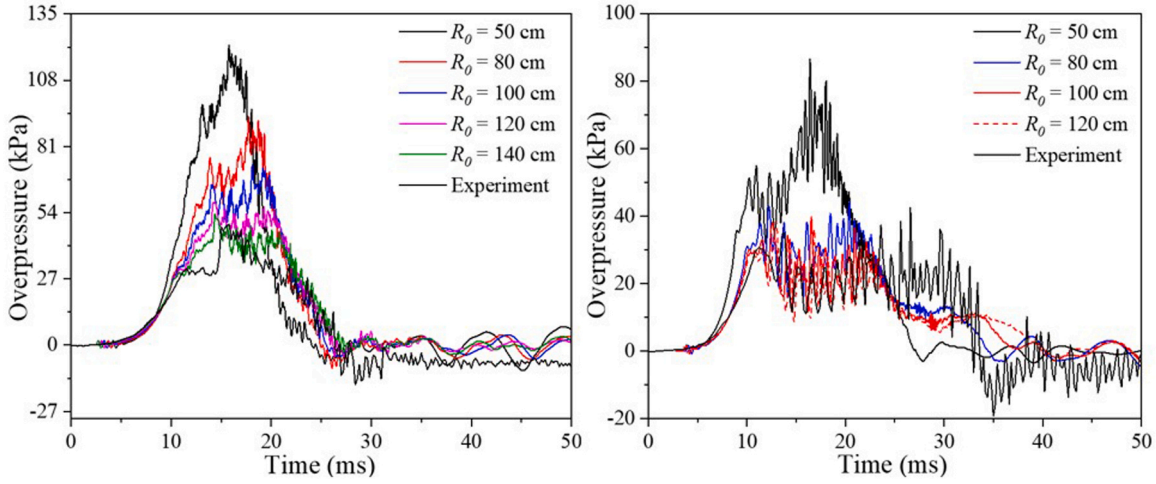

Fig. 17. Internal overpressure-time profiles vs. R_0 for rear ignition (left) and center ignition (right).

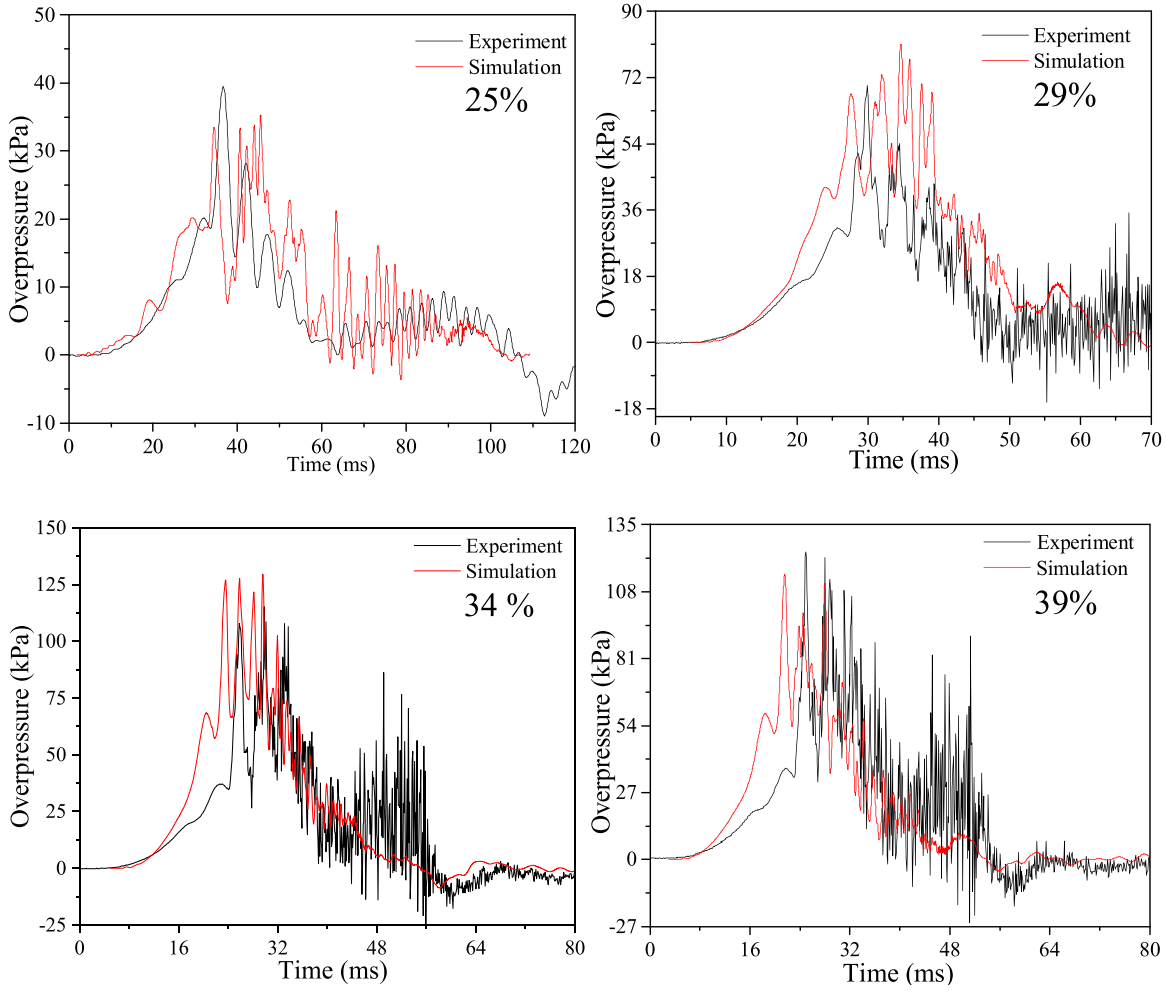

Fig. 18. Comparison of predicted overpressure-time curves and experimental data (Wang et al. 2018) for vented hydrogen explosion in a 1 m^3 container.

gas venting. As a result, the external overpressure-time profiles predicted using the LES turbulence model precede those predicted using k-ε, SST-ko, and DES turbulence models.

Fig. 7 compares predicted overpressure histories with and without consideration of heat transfer. Unlike the simulation results of a 20 L sphere explosion of methane-air mixture (Lei et al., 2022), it is observed that heat transfer and water condensation have a minimal effect on the overpressure-time curves in the context of vented hydrogen explosions for low vent coefficient. The maximum internal overpressure predicted in the adiabatic simulation is only slightly larger than the overpressure predicted when considering heat transfer and steam condensation. This can be explained by the fact that the chemical reaction rate of

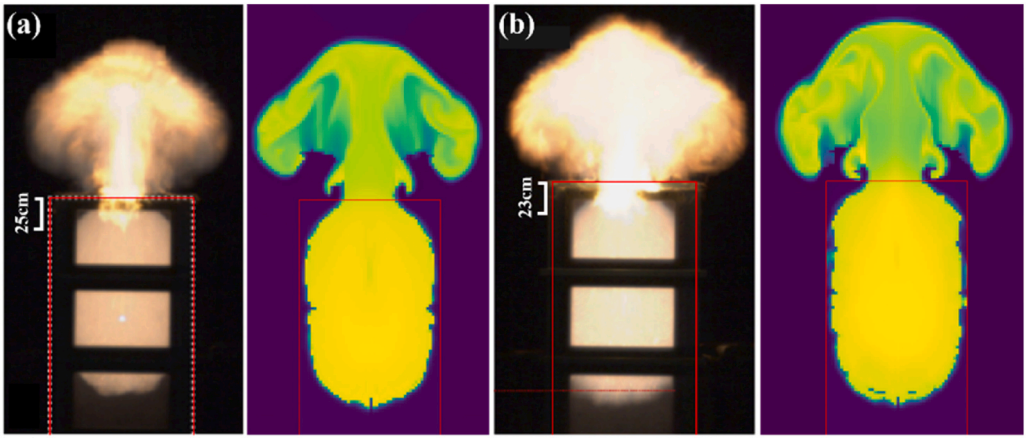

Fig. 19. Comparison of the typical flame behavior between the simulation results and experimental data of Wang et al. (2018) (Left: 29 % hydrogen-air mixtures, right: 34 % hydrogen-air mixtures).

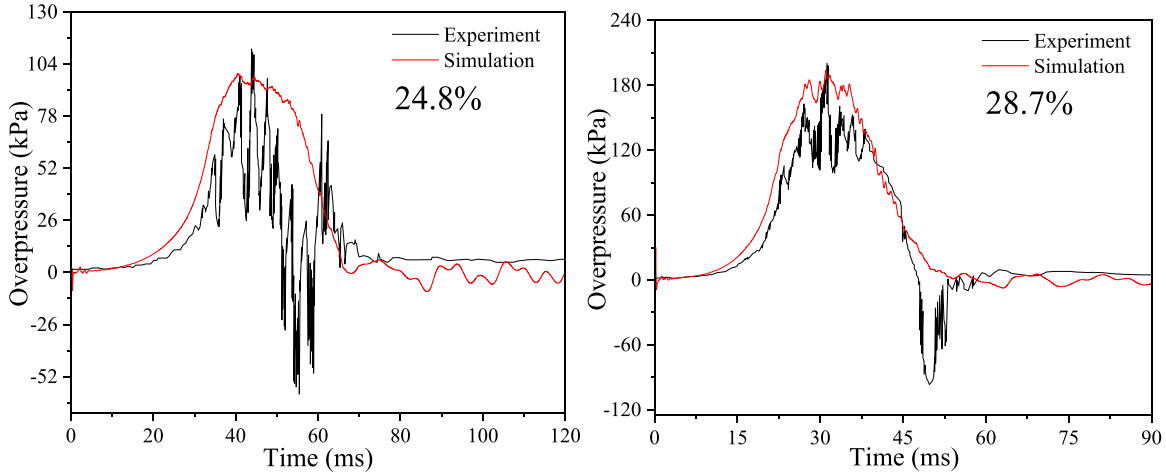

Fig. 20. Comparison between the predicted overpressure-time profiles(Daubech et al. 2013) and experimental data for 24.8 % hydrogen-air mixtures (left) and 28.7 % hydrogen-air mixtures (right).

hydrogen-air mixtures is higher than that of methane-air mixtures. Additionally, a portion of the high-temperature combustion product generated inside the vessel is rapidly expelled outside after vent rupture in vented explosions.

Fig. 8 depicts the heat transfer time curves induced by thermal radiation and convection, respectively. It is observed that heat loss does not occur due to radiation and convection before vent rupture. The small heat transfer of about 110 J induced by thermal radiation contributes to the slight difference in the maximum internal overpressure predicted by the adiabatic simulation compared to that considering heat transfer. However, convective heat transfer occurs after the maximum internal overpressure is reached.

To assess the performance of GASFLOW in simulating vented hydrogen deflagrations with different hydrogen concentrations and ignition locations, it is crucial to investigate the effect of grid size on the simulation results. Fig. 9 displays the overpressure-time curves predicted using different grid sizes for 30 % hydrogen-air mixtures in the case of rear ignition. The maximum internal overpressure demonstrates a decrease with the decrease of grid size. Obtaining grid-independent resolutions for high-speed hydrodynamic problems with strong coupling between combustion and turbulence can be challenging (Tolias et al., 2018; Vyazmina and Jallais, 2016; Wang et al., 2016). However, the maximum external overpressure shows a convergence trend with the decrease in grid size. In Fig. 9, the calculated maximum internal overpressure is slightly lower than the experimental data for a 0.77 cm grid, while it is slightly higher than the experimental data for a 1 cm grid. From a conservative standpoint, 1 cm cuboid grid in core domain was selected to validate the ability of GASFLOW-MPI in simulating vented hydrogen-air mixtures with different hydrogen concentrations and ignition locations.

Fig. 10 illustrates the comparison of predicted overpressure histories and experimental data for different hydrogen concentrations with rear ignition. It is observed that the predicted overpressures agree well with the experimental data, accurately capturing the two main overpressure peaks induced by vent rupture and external explosion, respectively. This agreement indicates that the simulation results effectively reproduce the experimental observations for varying hydrogen concentrations and rear ignition scenarios.

Fig. 11 depicts the comparison of predicted overpressure histories and experimental data for different hydrogen concentrations with center ignition. For the low hydrogen concentration of 22 %, the experimental data's maximum overpressure is larger than that of the predicted data. This discrepancy can be attributed to the fact that the maximum overpressure results from the interaction between combustion waves and acoustic waves of the vessel, constituting fluid-solid coupling. GASFLOW-MPI does not account for the interaction between fluid flow and structure, leading to a mismatch at lower hydrogen concentrations. Nevertheless, the predicted overpressure time profiles exhibit good agreement with experimental data as the hydrogen concentration exceeds 26 %.

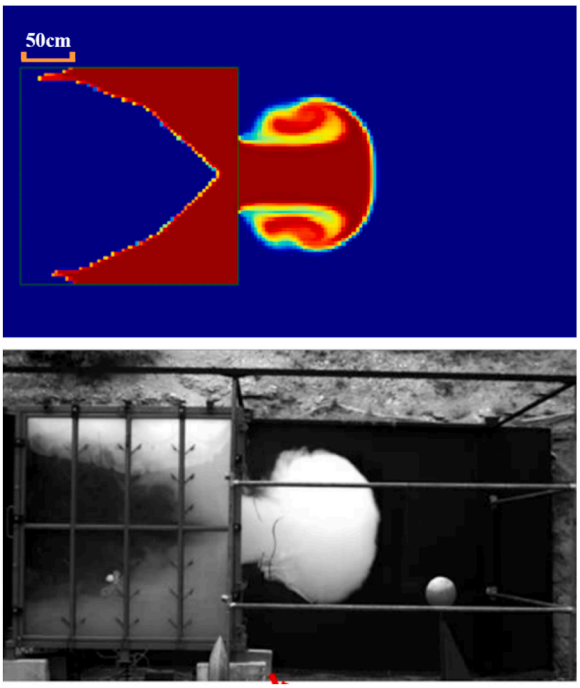

Fig. 21. Comparison of the typical unburned hydrogen-air mixture between the simulation results and experimental data of Daubech et al. (2013).

In Fig. 12, the variation of the maximum internal overpressure with hydrogen concentration is presented for both center and rear ignitions. With the exception of low hydrogen concentration in the case of center ignition, the predicted maximum overpressure aligns well with the experimental data, particularly in the case of rear ignition.

External explosion is a critical phenomenon in vented hydrogen explosions due to the wide flammable limit of hydrogen-air mixtures. The maximum internal overpressure becomes increasingly influenced by external explosion with the increase of hydrogen concentration, especially for rear ignition, as depicted in Fig. 10 and Fig. 11. Therefore, it is imperative to assess the performance of GASFLOW-MPI in simulating external overpressure-time profiles.

Fig. 13 presents the comparison of typical external overpressure-time curves between experimental data and simulation results for 34 % and 38 % hydrogen-air mixtures for rear ignition. The simulated overpressure-time curves agree well with the experimental data while the predicted maximum external overpressures are slightly lower than the experimental values. In Fig. 14, turbulence intensity (u′), hydrogen concentration, and flame venting rate at the time of flame venting are displayed for different hydrogen concentrations. Higher turbulence intensity is induced near the vent's edge and around the first pressure monitoring rod. The flame venting rate is approximately 460 m/s, 595 m/s, and 590 m/s for 30 %, 34 %, and 38 % hydrogen-air mixtures, respectively. The flame venting rate is primarily related to the chemical reaction rate, with its maximum value occurring at a slightly fuel-rich hydrogen-air mixture (Jo and Crowl, 2009).

Fig. 15 shows the external overpressure-time curves and corresponding turbulence intensity (u′) time curves. The value of u′ is about 6.26 m/s, 8.04 m/s, and 4.84 m/s at the maximum external overpressure for 30 %, 34 %, and 38 % hydrogen-air mixtures, respectively. External explosion is a deflagration process with strong initial turbulence. In Fig. 16, the external hydrogen volume fraction during the formation of the maximum external overpressure is depicted. It is evident that more unburned mixture participates in external chemical reaction for 38 % hydrogen-air mixture. Although the flame venting rates are nearly identical for 34 % and 38 % hydrogen-air mixtures, the maximum external overpressure for 38 % hydrogen-air mixture is larger than that for 34 % hydrogen-air mixture. The maximum external overpressure is influenced by the flame venting rate, turbulence intensity, and the volume of hydrogen participating in reaction. Therefore, the maximum external overpressure for 38 % hydrogen-air mixture is slightly larger than those for 30 % and 34 % hydrogen-air mixtures.

Given the significance of explosion venting in engineering applications, it is necessary to assess the performance of GASFLOW-MPI in simulating vented hydrogen-air explosions in medium-scale containers. Prior to conducting numerical simulations of medium-scale vented hydrogen explosions, the effect of R_0 on the overpressure-time profiles was investigated.

Fig. 17 illustrates the changes of internal overpressure-time profiles with R_0 for rear and center ignitions. It is observed that the maximum internal overpressure decreases with R_0 for rear ignition. However, the maximum internal overpressure converges as R_0 decreases to $R_0 =$ 100 cm for center ignition, which is twice the maximum distance of flame propagation inside the vessel. In Fig. 10 and Fig. 12, the predicted maximum internal overpressure for rear ignition is slightly lower than the experimental data, except for the 30 % hydrogen-air mixture. Therefore, the predicted maximum internal overpressure increases as R_0 decreases from $R_0 = 120$ cm to $R_0 = 100$ cm. In other words, the predicted results align more closely with the experimental data. Consequently, the value of R_0 is selected as twice the maximum distance of flame propagation inside the vessel for simulating medium-scale vented hydrogen explosions.

In the current study, experiments involving medium-scale vented hydrogen explosions conducted within a 1 m^3 vessel and a 4 m^3 container were selected. (Daubech et al., 2013; Wang et al., 2018). The assessment, as illustrated in Fig. 18, compare the maximum internal overpressure-time curves derived from simulation results against experimental data for hydrogen-air mixtures ranging from 25 % to 39 % (Wang et al., 2018). The agreement between the predicted results and experimental data is obtained for conditions associated with both fuel-lean and fuel-rich hydrogen-air mixtures. Although the maximum internal overpressure predicted for the 34 % hydrogen-air mixture exceeds the corresponding experimental observation, the error is only about 13 %. Furthermore, Fig. 19 presents the comparison between predicted results and experimental observations of typical flame behavior, which enhances the credibility of the computational simulations. Fig. 20 shows a comparative evaluation of overpressure-time build-up for hydrogen-air mixtures at concentrations of 24.8 % and 28.7 %, corresponding experiments conducted in a 4 m^2 container (Daubech et al., 2013). The evolution of typical unburned hydrogen-air mixture distribution during vented hydrogen explosion is shown in Fig. 21. Collectively, these rigorous comparisons validate the performance of GASFLOW-MPI in simulating medium-scale vented hydrogen explosions.

7. Conclusion

In the current study, numerical simulation of vented hydrogen explosions was performed utilizing the computational fluid dynamics (CFD) software GASFLOW-MPI. A turbulent combustion model based on Schimdt correlation was developed, incorporating two intrinsic flame instabilities. Simulation results revealed that the internal overpressure preceding vent rupture is primarily influenced by the laminar flame speed. Notably, Large Eddy Simulation (LES) turbulence tended to overestimate turbulence intensity, resulting in higher overpressure predictions compared to RANS k-ε, SST k-ω, and DES turbulence models. The rapid chemical reaction and the venting of combustion products mitigated the impact of heat transfer on internal overpressure. External explosion, characterized by strong initial turbulence and jet flame ignition, manifested as a deflagration process. The peak of external overpressure corresponded to the complete consumption of expelled unburned mixture. The magnitude of the maximum external overpressure was associated with factors such as flame venting rate,

turbulence intensity, and the volume of hydrogen participating chemical reaction. Except for cases involving low hydrogen concentration in center ignition, the predicted overpressure histories agree well with experimental data across various hydrogen concentrations in both center and rear ignitions. Furthermore, the competency of GASFLOW in simulating medium-scale vented hydrogen scenarios was substantiated through validation exercises.

CRediT authorship contribution statement

Mike Kuznetsov: Methodology, Investigation, Conceptualization. **Thomas Jordan:** Supervision, Conceptualization. **shengchao rui:** Writing – review & editing, Writing – original draft, Methodology, Investigation, Formal analysis, Data curation, Conceptualization. **Jianjun Xiao:** Supervision, Resources, Methodology. **Changjian Wang:** Supervision, Data curation. **Fangnian Wang:** Software, Conceptualization.

Declaration of Competing Interest

We declare that we do not have any interest that represents a conflict of interest in connection with the work submitted.

Acknowledgement

This work was performed on the HoreKa supercomputer funded by the Ministry of Science, Research and the Arts Baden-Wrttemberg and by the Federal Ministry of Education and Research, Germany.

References

Arntzen, B.J., 1998. Modeling of Turbulence and Combustion for Simulation of Gas Explosions in Complex Geometries., in: Arntzen, B.J. (Ed.), PhD Thesis. Norwegian University of Science and Technology, Division of Applied Mechanics, Thermodynamics and Fluid Dynamics.

Bauwens, C., Chaffee, J., Dorofeev, S., 2010. Effect of ignition location, vent size, and obstacles on vented explosion overpressures in propane-air mixtures. Combust. Sci. Technol. 182, 1915–1932.

Bauwens, C.R., Chaffee, J., Dorofeev, S.B., 2011. Vented explosion overpressures from combustion of hydrogen and hydrocarbon mixtures. Int. J. Hydrog. Energy 36, 2329–2336.

Bauwens, C.R., Chao, J., Dorofeev, S.B., 2012a. Effect of hydrogen concentration on vented explosion overpressures from lean hydrogen–air deflagrations. Int. J. Hydrog. Energy 37, 17599–17605.

Bauwens, C.R., Chao, J., Dorofeev, S.B., 2012b. Evaluation of a multi peak explosion vent sizing methodology, International symposium on hazard, prevention and mitigation of industrial explosions.

Bauwens, C.R., Dorofeev, S.B., 2014. Effect of initial turbulence on vented explosion overpressures from lean hydrogen–air deflagrations. Int. J. Hydrog. Energy 39, 20509–20515.

Bauwens, C.R.L., Bergthorson, J.M., Dorofeev, S.B., 2019. Modeling the formation and growth of instabilities during spherical flame propagation. Proc. Combust. Inst. 37, 3669–3676.

Bird, R., Stewart, W., Lightfoot, E., 1960. Transport phenomena.

Bradley, D., Lawes, M., Liu, K., Mansour, M.S., 2013. Measurements and correlations of turbulent burning velocities over wide ranges of fuels and elevated pressures. Proc. Combust. Inst. 34, 1519–1526.

Bray, K., 1990. Studies of the turbulent burning velocity. Math., Phys. Eng. Sci. 431, 20.

Cao, W.G., Li, W.J., Yu, S., Zhang, Y., Shu, C.M., Liu, Y.F., Luo, J.W., Bu, L.T., Tan, Y.X., 2021. Explosion venting hazards of temperature effects and pressure characteristics for premixed hydrogen-air mixtures in a spherical container. Fuel 290.

Chandrasekhar, S., 1960. Radiative transfer. Dover Publications, New York.

Chen, Y., Li, Y., Li, Z., Ji, C., Liu, X., 2020. Experimental studies on external pressures during vented lean hydrogen deflagrations in a 27 m3 chamber. Process Saf. Environ. Prot. 139, 334–340.

Daubech, J., Proust, C., Gentilhomme, O., Jamois, C., Mathieu, L., 2013. Hydrogen–air vented explosions: new experimental data, 5th International Conference on Hydrogen Safety, Brussels, Belgium.

David, W., 1942. Radiation from flames. Nature 150, 407–408.

Guo, J., Sun, X.X., Rui, S.C., Cao, Y., Hu, K.L., Wang, C.J., 2015. Effect of ignition position on vented hydrogen–air explosions. Int. J. Hydrog. Energy 40, 15780–15788.

Hadjipanayis, M., Beyrau, F., Lindstedt, R., Atkinson, G., Cusco, L., 2015. Thermal radiation from vapour vloud explosions. Process Saf. Environ. Prot. 94, 517–527.

Hisken, H., Atanga, G., Lakshmipathy, S., 2016. Validating, documenting and qualifying models used for consequence assessment of hydrogen explosion scenarios. 11th International symposium on hazards, prevention and mitigation of industrial explosions, 24-29.

ISSA, R.I., 1985. Solution of the implicitly discretised fluid flow equations by operator-splitting. J. Comput. Pyhsics 62, 40–65.

Jo, Y.D., Crowl, D.A., 2009. Explosion characteristics of hydrogen-air mixtures in a spherical vessel. Process Saf. Prog. 29, 216–223.

Kumar, R.K., 2006. Vented combustion of hydrogen-air mixtures in a large rectangular volume. 44th AIAA Aerosp. Sci. Meet. Exhib., Reno, Nev., USA.

Kuznetsov, M., Friedrich, A., Stern, G., Kotchourko, N., Jallais, S., L'Hostis, B., 2015. Medium-scale experiments on vented hydrogen deflagration. J. Loss Prev. Process Ind. 36, 416–428.

Lakshmipathy, S., Skjold, T., Hisken, H., Atanga, G., 2019. Consequence models for vented hydrogen deflagrations: CFD vs. engineering models. Int. J. Hydrog. Energy 44, 8699–8710.

Landau, L.D., 1944. On the Theory of Slow Combustion. Acta PhysicochimicaURSS 19, 77–85.

Lei, B., Xiao, J., Kuznetsov, M., Jordan, T., 2022. Effects of heat transfer mechanism on methane-air mixture explosion in 20 L spherical device. J. Loss Prev. Process Ind. 80.

Lewis, B., von Elbe, G., 1987. Combustion, Flames and Explosion of Gases. Academic Press, New York.

Li, H.W., Tang, Z.S., Li, J.L., Guo, J., Zhang, J.Q., Li, Q., 2019. Investigation of vented hydrogen-air deflagrations in a congested vessel. Process Saf. Environ. Prot. 129, 196–201.

Madhav Rao Vendra, C., Wen, J.X., 2019. Numerical modelling of vented lean hydrogen deflagations in an ISO container. Int. J. Hydrog. Energy 44, 8767–8779.

Mogi, T., Matsunaga, T., Dobashi, R., 2017. Propagation of blast waves from a bursting vessel with internal hydrogen-air deflagration. Int. J. Hydrog. Energy 42, 7683–7690.

Molkov, V., Bragin, M., 2015. Hydrogen–air deflagrations: vent sizing correlation for low-strength equipment and buildings. Int. J. Hydrog. Energy 40, 1256–1266.

Molkov, V.V., 2012. hydrogen safety engineering. Fundamentals.

Rui, S., Wang, C., Luo, X., Jing, R., Li, Q., 2021. External explosions of vented hydrogen-air deflagrations in a cubic vessel. Fuel 301.

Rui, S., Wang, Q., Wang, C., Zhang, A., 2024. Effects of ignition location and vent area on the external explosion in vented hydrogen explosions. Process Saf. Environ. Prot. 183, 602–616.

Schmid, H., Habisreuther, P., Leuckel, W., 1998. A model for calculating heat release in premixed turbulent flames. Combust. Flame 113, 79–91.

Siegel, R., Howell, J., 1992. Thermal radiation heat transfer. Hemisphere Publishing, Washington.

Sinha, A., Madhav Rao, V.C., Wen, J.X., 2019. Performance evaluation of empirical models for vented lean hydrogen explosions. Int. J. Hydrog. Energy 44, 8711–8726.

Sinha, A., Wen, J.X., 2019. A simple model for calculating peak pressure in vented explosions of hydrogen and hydrocarbons. Int. J. Hydrog. Energy 44, 22719–22732.

Skjold, T., Hisken, H., Lakshmipathy, S., Atanga, G., Bernard, L., van Wingerden, M., Olsen, K.L., Holme, M.N., Turøy, N.M., Mykleby, M., van Wingerden, K., 2019. Vented hydrogen deflagrations in containers: effect of congestion for homogeneous and inhomogeneous mixtures. Int. J. Hydrog. Energy 44, 8819–8832.

Sparrow, E., Cess, R., 1978. Radiation heat transfer. Hemisphere Publishing, Washington.

Tolias, I.C., Stewart, J.R., Newton, A., Keenan, J., Makarov, D., Hoyes, J.R., Molkov, V., Venetsanos, A.G., 2018. Numerical simulations of vented hydrogen deflagration in a medium-scale enclosure. J. Loss Prev. Process Ind. 52, 125–139.

Tolias, I.C., Venetsanos, A.G., 2018. An improved CFD model for vented deflagration simulations – analysis of a medium-scale hydrogen experiment. Int. J. Hydrog. Energy 43, 23568–23584.

Tolias, I.C., Venetsanos, A.G., Markatos, N., Kiranoudis, C.T., 2014. CFD modeling of hydrogen deflagration in a tunnel. Int. J. Hydrog. Energy 39, 20538–20546.

Tolias, I.C., Venetsanos, A.G., Markatos, N., Kiranoudis, C.T., 2017. CFD evaluation against a large scale unconfined hydrogen deflagration. Int. J. Hydrog. Energy 42, 7731–7739.

Tolias, I.C., Venetsanos, A.G., Markatos, N.C., Kiranoudis, C.T., 2015. CFD simulation of hydrogen deflagration in a vented room. J. Phys.: Conf. Ser.

Ugarte, O.J., Akkerman, Vy, Rangwala, A.S., 2016. A computational platform for gas explosion venting. Process Saf. Environ. Prot. 99, 167–174.

Vyazmina, E., Jallais, S., 2016. Validation and recommendations for FLACS CFD and engineering approaches to model hydrogen vented explosions: Effects of concentration, obstruction vent area and ignition position. Int. J. Hydrog. Energy 41, 15101–15109.

Wang, J., Guo, J., Yang, F., Zhang, J., Lu, S., 2018. Effects of hydrogen concentration on the vented deflagration of hydrogen-air mixtures in a 1m^{3}vessel. Int. J. Hydrog. Energy 43, 21161–21168.

Wang, Q., Luo, X., Wang, C., Liu, Y., Zhou, P., Li, B., 2022. Experimental study on external explosion for vented hydrogen deflagration in a rectangular tube with different vent coefficients. Process Saf. Environ. Prot. 158, 331–339.

Wang, Y., Lian, Z., Zhang, Q., 2016. Effect of Ignition Location and Vent on Hazards of Indoor Liquefied Petroleum Gas Explosion. Combust. Sci. Technol. 189, 698–716. Xiao, J., Breitung, W., Kuznetsov, M., Zhang, H., 2017a. Numerical investigations of turbulent slow deflagration of premixed H2-air-H2O mixture in THAI test HD-22

using CFD code GASFLOWMPI. 17th international topical meeting on nuclear reactor thermal hydraulics (NURETH-17).

Xiao, J., Breitung, W., Kuznetsov, M., Zhang, H., Travis, J.R., Redlinger, R., Jordan, T., 2017b. GASFLOW-MPI: A new 3-D parallel all-speed CFD code for turbulent dispersion and combustion simulations Part II: First analysis of the hydrogen explosion in Fukushima Daiichi Unit 1. Int. J. Hydrog. Energy 42, 8369–8381.

Xiao, J., Breitung, W., Kuznetsov, M., Zhang, H., Travis, J.R., Redlinger, R., Jordan, T., 2017c. GASFLOW-MPI: a new 3-D parallel all-speed CFD code for turbulent dispersion and combustion simulations. Part I: models, verification and validation. Int. J. Hydrog. Energy 42, 8346–8368.

Xiao, J., Kuznetsov, M., Travis, J.R., 2018. Experimental and numerical investigations of hydrogen jet fire in a vented compartment. Int. J. Hydrog. Energy 43, 10167–10184.

Xiao, J., Travis J.R., Royl P., Necker G., Svishchev A., T., J., 2016a. GASFLOW-MPI: a scalable computational fluid Dynamics code for gases, aerosols and combustion. Theory and computational model (revision 1.0). Theory and computational model (revision 1.0).KIT Scientific Publishing; In: Volume 1.

Xiao, J., Travis, J.R., Royl, P., Necker, G., Svishchev, A., Jordan, T., 2016b. Three-dimensional all-speed CFD code for safety analysis of nuclear reactor containment: Status of GASFLOW parallelization, model development, validation and application. Nucl. Eng. Des. 301, 290–310.

Xu, J., Chen, X., Jiang, H., Gao, W., 2022. Vented hydrogen-air explosions at elevated static activation pressures. Process Saf. Environ. Prot. 168, 474–486.

Zhang, H., Li, Y., Xiao, J., Jordan, T., 2018a. Detached Eddy Simulation of hydrogen turbulent dispersion in nuclear containment compartment using GASFLOW-MPI. Int. J. Hydrog. Energy 43, 13659–13675.

Zhang, H., Li, Y., Xiao, J., Jordan, T., 2018b. Large eddy simulations of the all-speed turbulent jet flow using 3-D CFD code GASFLOW-MPI. Nucl. Eng. Des. 328, 134–144.

Zhang, K., Du, S., Chen, H., Wang, J., Zhang, J., Guo, Y., Guo, J., 2022. Effect of hydrogen concentration on the vented explosion of hydrogen–air mixtures in a 5-m-long duct. Process Saf. Environ. Prot. 162, 978–986.

Zhang, Y., Chen, R., Zhao, M., Luo, J., Feng, W., Fan, W., Tan, Y., Cao, W., Shu, C.-M., Yu, C., 2020. Hazard evaluation of explosion venting behaviours for premixed hydrogen-air fuels with different bursting pressures. Fuel 268.